J|A|C|S
ARTICLES
Published on Web 09/06/2002

What Factors Affect the Regioselectivity of Oxidation by Cytochrome P450? A DFT Study of Allylic Hydroxylation and Double Bond Epoxidation in a Model Reaction

Sam P. de Visser, François Ogliaro, Pankaz K. Sharma, and Sason Shaik*

Contribution from the Department of Organic Chemistry and The Lise Meitner-Minerva Center for Computational Quantum Chemistry, The Hebrew University of Jerusalem, 91904 Jerusalem, Israel

Received May 12, 2002

Abstract: Epoxidation (C═C) vis-à-vis allylic hydroxylation (C−H) reactions of propene with a model compound I (Cpd I) of the enzyme cytochrome P450 were studied using B3LYP density functional theory. Potential energy profiles and kinetic isotope effects (KIE) were calculated. The interactions in the protein pocket were mimicked by adding two external NH- - -S hydrogen bonds to the thiolate ligand and by introducing a nonpolar medium (with a dielectric constant, $\epsilon = 5.7$) that can exert a polarization effect on the reacting species. A two-state reactivity (TSR) with high-spin (HS) and low-spin (LS) states were located for both processes (Ogliaro, F.; Harris, N.; Cohen, S.; Filatov, M.; de Visser, S. P.; Shaik, S. *J. Am. Chem. Soc.* **2000**, *122*, 8977−8989. de Visser, S. P.; Ogilaro, F.; Harris, N.; Shaik, S. *J. Am. Chem. Soc.* **2001**, *123*, 3037−3047). The HS processes were found to be stepwise, whereas the LS processes were characterized as nonsynchronous but effectively concerted pathways. The computed KIE for C−H hydroxylation with and without tunneling corrections are large (>7), and they support the assignment of the corresponding transition states as hydrogen-abstraction species (Groves, J. T.; Han, Y.-Z. In *Cytochrome P450: Structures, Mechanism and Biochemistry*, 2nd ed.; Ortiz de Montellano, P. R., Ed.; Plenum Press: New York, 1995; Chapter 1; pp 3−48). In the gas phase, epoxidation is energetically favorable by 3.4 kcal mol^{-1}. Inclusion of zero-point energy reduces this difference but still predicts C═C/C−H > 1. Environmental effects were found to have major impact on the C═C/C−H ratio as well as on the stereoselectivity of the processes. Thus, *two NH- - -S hydrogen bonds away from the reaction center* reverse the regioselectivity and prefer hydroxylation, namely, C═C/C−H <1. The polarity of the medium further accentuates the trend and leads to a change by 2 orders of magnitude in the regioselectivity, C═C/C−H $\ll$ 1. Furthermore, since the environmental interactions prefer the LS over the HS reactions, both hydroxylation and epoxidation processes are rendered more stereoselective, again by 2 orders of magnitude. It follows, therefore, that *Cpd I is a chameleon oxidant* (Ogliaro, F.; Cohen, S.; de Visser, S. P.; Shaik, S. *J. Am. Chem. Soc.* **2000**, *122*, 12892−12893; Ogliaro, F.; de Visser, S. P.; Cohen, S.; Kaneti, J.; Shaik, S. *Chembiochem.* **2001**, *2*, 848−851; Ogliaro, F.; de Visser, S. P.; Groves, J. T.; Shaik, S. *Angew. Chem., Int. Ed.* **2001**, *40*, 2874−2878) *that tunes its reactivity and selectivity patterns in response to the protein environment in which it is accommodated*. A valence bond (VB) model, akin to "redox mesomerism" (Bernadou, J.; Fabiano, A.-S.; Robert, A.; Meunier, B. *J. Am. Chem. Soc.* **1994**, *116*, 9375−9376), is constructed and enables the description of a chameleon transition state. It shows that the good donor ability of the thiolate ligand and the acceptor ability of the iron porphyrin create mixed-valent situations that endow the transition state with a great sensitivity to external perturbations as in the protein pocket. The model is used to discuss the computed results and to relate them to experimental findings.

1 Introduction.

C−H hydroxylation and C═C epoxidation are among the most important reactions catalyzed by the super-family of cytochrome P450 enzymes (P450).[1−11] The ability of the enzyme to hydroxylate nonactivated C−H bonds, and to do so with high stereoselectivity, is a feat that can be achieved by only very few electrophilic reagents from among the huge arsenal available in chemistry. P450 can also epoxidize alkenes usually with high stereoselectivity.[1a,4] This, however, is expected since, generally, double bonds are more easily oxygenated by electrophilic reagents than are C−H bonds.[12] An intriguing aspect is the capability of P450 to perform allylic C−H hydroxylation in the presence of the intrinsically more reactive double bond moiety, Scheme 1a.

The regioselectivity of C−H hydroxylation versus C═C epoxidation varies widely and appears to depend on a complex mixture of factors: the substrate, its isotopic substitution, the

* To whom correspondence should be addressed. E-mail: sason@yfaat.ch.huji.ac.il.

Scheme 1. Competing Epoxidation and Allylic Hydroxylation in the Reaction of Compound I (Cpd I) with an Alkene[a]

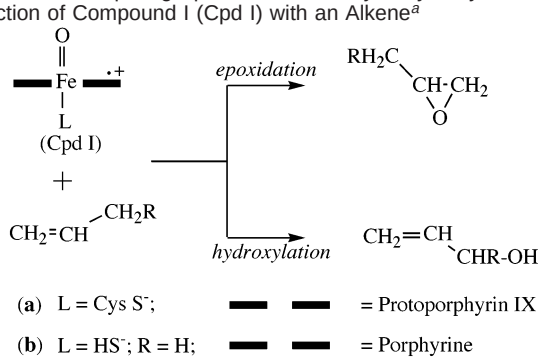

[a] (a) Specifies the proximal ligand and the porphyrin macrocycle in case of the enzyme. (b) Specifies the model Cpd I species and propene used in the theoretical study.

specific P450 isozyme, as well as noncovalent interactions exerted in the protein pocket on the proximal cysteinate ligand, for example, hydrogen bonding of the type NH- - -S. Thus, for example, the oxidation reaction of cyclohexene by $P450_{LM2}$ (rat liver microsomal enzyme) produces cyclohexene oxide and 2-cyclohexen-1-ol in almost equal amounts.[13] This ratio increases to 4.7 after substitution of cyclohexene with four deuterium atoms leading to 3,3,6,6-tetradeuteriocyclohexene.[14] Groves et al.[14] showed that a synthetic analogue of the active species of P450, compound I (Cpd I), reacts with cyclohexene to produce cyclohexene oxide and cyclohexen-3-ol in a ratio of 14:1. Subsequently,[15] it was demonstrated that these competing reactions proceed via independent pathways and that the ratio of epoxidation to hydroxylation depends on the identity of the proximal ligand (L, Scheme 1) in the Cpd I species, as well as on the temperature.

Mansuy et al.[12] used synthetic analogues of Cpd I, and showed that electron-withdrawing substituents on the porphyrin ring generally increased the ratio of C−H hydroxylation to C=C epoxidation. Nagano et al.[16] showed that the high C=C/C−H reaction ratio depended on the identity of the proximal ligand in Cpd I, such that P450 with the cysteinate ligand (L = $CysS^-$), gave higher yields of C−H hydroxylation, compared with synthetic reagents that possess a variety of other ligands (e.g, Cl^-, imidazole, water, etc.). Mansuy et al.[12] followed by Nagano et al.[16] ascribed the increase in the yields of C−H hydroxylation to the extent of radical character on the iron−oxo moiety of Cpd I, that is, as Fe−O•, as a result of changing porphyrin substituents or proximal ligand. It was argued that electron-withdrawing substituents on porphyrin and proximal ligands that are good electron donors (e.g., $CysS^-$) increase the radical character (Fe−O•) of the iron−oxo moiety of Cpd I, and thereby facilitate C−H hydroxylation. Thus, this approach views the changes of C=C/C−H regioselectivity arising due to an electronic effect associated with the variable electrophilic and radicalar characters of Cpd I. This view of Cpd I is akin to the general idea termed "redox mesomerism",[17] in which the proximal ligand can participate in electron delocalization into the iron center and the porphyrin "hole".[1a,3,4]

The protein pocket and the interactions it applies on a given system[1b] also play a role in affecting the regioselectivity. Thus, a study by Ruettinger and Fulco[18] using $P450_{BM3}$, showed that a series of closely related fatty acids gave C=C/C−H regioselectivitites that ranged from 0.53 to 0.007. These results were interpreted in terms of the conformation of substrate binding, the juxtaposition of the substrate moieties vis-à-vis the active species, and stereoelectronic effects due to the substrate. Studies by Suzuki et al.[19] and a more recent one by Morishima et al.[20] highlighted the role of NH- - -S hydrogen bonding to the thiolate ligand. Morishima et al. showed that severing the NH- - -S bond due to the amino acid residue Leu358 in $P450_{cam}$ favored C=C epoxidation of cyclohexene. The authors ascribed the changes of the C=C/C−H ratio to the variable electrophilic and radicalar characters of Cpd I, which was modulated by the NH- - -S bonding. However, since severing the NH- - -S hydrogen bond imparted by Gln360 was found to have an adverse effect on the integrity of the binding site, the mutation might bring about a mixed bag of factors.[21]

As opposed to the above studies, which focused on Cpd I as the sole oxidant, Vaz et al.[22] invoked the interplay of two oxidants, Cpd I and its ferric peroxide precursor (Cpd 0): Cpd I leads to more C−H hydroxylation, while Cpd 0 leads to more C=C epoxidation. Vaz et al.[22] studied the reactions of $P450_{2B4}$ and $P450_{2E1}$ enzymes and their mutants (T → A mutants) with *cis*- and *trans*-butenes and cyclohexene and observed both epoxidation and allylic C−H hydroxylations. In the case of cyclohexene all P450 enzymes gave almost invariant epoxide/alkenol product ratios in the range of 1.0−2.4, while the 2-butenes gave highly variable ratios in the range 4 → 462. It was argued that since the mutation affected the proton relay mechanism that converted Cpd 0 to Cpd I, it also affected the amounts of the two oxidation species[9] and hence also the C=C/C−H oxygenation ratio.

(1) Ortiz de Montellano, P. R., Ed. *Cytochrome P450: Structures, Mechanism and Biochemistry*, 2nd ed.; Plenum Press: New York, 1995; in particular the following chapters: (a) Groves, J. T.; Han, Y.-Z. Chapter 1, pp 3−48. (b) Mueller, E. J.; Loida, P. J.; Sligar, S. G. Chapter 3, pp 83−124. (c) Ortiz de Montellano, P. R. Chapter 8, pp 245−304..
(2) Kadish, K. M., Smith, K. M., Guilard, R., Eds. *The Porphyrin Handbook*; Academic Press: San Diego, 2000. In particular the following chapters: (a) Mansuy, D.; Battioni, P. Chapter 26, Vol. 4, p 1. (b) Groves, J. T.; Shalyaev, K.; Lee, J. Chapter 27, Vol. 4, p 17. (c) Suslick, K. S. Chapter 28, Vol. 4, p 41. (d) Watanabe Y. Chapter 30, Vol. 4, p 97. (e) Meunier, B.; Robert, A.; Pratviel, G.; Bernadou, J. Chapter 31, Vol. 4, p 119.
(3) Sono, M.; Roach, M. P.; Coulter, E. D.; Dawson, J. H. *Chem. Rev.* **1996**, *96*, 2841.
(4) Woggon, W.-D. *Top. Curr. Chem.* **1996**, *184*, 40.
(5) Woggon, W.-D.; Wagenknecht, H. A.; Claude, C. *J. Inorg. Biochem.* **2001**, *83*, 289−300.
(6) Meunier, B. *Chem. Rev.* **1992**, *92*, 1411.
(7) Meunier, B.; Bernadou, J. *Struct. Bonding* **2000**, *97*, 1−35.
(8) Ostovic, D.; Bruice, T. C. *Acc. Chem. Res.* **1992**, *25*, 314.
(9) Newcomb, M.; Toy, P. H. *Acc. Chem. Res.* **2000**, *33*, 449.
(10) Ortiz de Montellano, P. R. *Trends Pharmacol. Sci.* **1989**, *10*, 354−359.
(11) Dolphin, D.; Traylor, T. G.; Xie, L. Y. *Acc. Chem. Res.* **1997**, *30*, 251−259.
(12) Bartoli, J. F.; Brigaud, O.; Battioni, P.; Mansuy, D. *J. Chem. Soc., Chem. Commun.* **1991**, 440−441.
(13) White, R. E.; Groves, J. T.; McClusky, G. A. *Acta Biol. Med. Germ.* **1979**, *38*, 475−482.
(14) Groves, J. T.; Subramanian, D. V. *J. Am. Chem. Soc.* **1984**, *106*, 2177.
(15) Groves, J. T.; Gross, Z.; Stern, M. K. In *Bioinorganic Chemistry: An Inorganic Perspective of Life*; Kessissoglon, D. P., Ed.; NATO Advanced Study Institute Series 459; Kluwer: Dordrecht, The Netherlands, 1995; pp 39−47.
(16) Ohno, T.; Suzuki, N.; Dokoh, T.; Urano, Y.; Kikuchi, K.; Hirobe, M.; Higuchi, T.; Nagano, T. *J. Inorg. Biochem.* **2000**, *82*, 123−125.
(17) Bernadou, J.; Fabiano, A.-S.; Robert, A.; Meunier, B. *J. Am. Chem. Soc.* **1994**, *116*, 9375−9376.
(18) Ruettinger, R. T.; Fulco, A. J. *J. Biol. Chem.* **1981**, *256*, 5728−5734.
(19) Suzuki, N.; Huguchi, T.; Urano, Y.; Kikuchi, K.; Uekusa, H.; Ohashi, Y.; Uchida, T.; Kitagawa, T.; Nagano, T. *J. Am. Chem. Soc.* **1999**, *121*, 11571−11572
(20) Yoshioka, S.; Takahashi, S.; Ishimori, K.; Morishima, I. *J. Inorg. Biochem.* **2000**, *81*, 141−151.
(21) Yoshioka, S.; Takahashi, S.; Hori, H.; Ishimori, K.; Morishima, I. *Eur. J. Biochem.* **2001**, *268*, 252−259.
(22) Vaz, A. D. N.; McGinnity, D. F.; Coon, M. J. *Proc. Natl. Acad. Sci. U.S.A.* **1998**, *95*, 3555.

An additional dimension of the problem is the variable stereoselectivity of C═C epoxidation, C−H hydroxylation, or both. Groves et al.[1a] have shown that, despite the high stereoselectivity, these reactions are not stereospecific and involve intermediates with finite lifetimes, which reveal their presence by rearrangement. Thus, allylic hydroxylation of cyclohexene and related substrate exhibits 20−40% allylic rearrangement due to migration of the double bond.[14] On the other hand, Woggon[4] reported that the allylic hydroxylation of geraniol by $P450_{cath}$ was fully stereospecific. Nevertheless, in both the cases, the kinetic isotope effects (KIE) for allylic hydroxylation were large (i.e., KIE = 8), suggesting that the transition states resembled hydrogen-abstraction transition states. Similar trends were also obtained for epoxidation, where stereospecific results ($P450_{2B1}$ and $P450_{2E1}$ with *cis*- and *trans*-butenes) were reported,[22] as well as side products that fit stepwise epoxidation (e.g., $P450_{LM2}$ with propene).[23] What are the reasons for the generally high but incomplete and variable stereoselectivity? And how does this feature differ for C−H hydroxylation vis-à-vis C═C epoxidation?

Clearly, the C═C/C−H competition in P450 oxygenation is a multidimensional complex problem that may benefit from the insight provided by theory. However, due to the complexity of the problem, such a study program must necessarily be conducted step by step. Herein, we use density functional theory (DFT), to focus on the *electronic factors* that affect C−H/C═C hydroxylation in the reaction of a model Cpd I with the smallest substrate, propene, that can in principle, exhibit both reactions, **(b)** in Scheme 1. The study characterizes the mechanisms and their regio- and stereoselectivities and determines semiclassical kinetic isotope effect (KIE) values corrected by tunneling for the C−H hydroxylation. To elucidate the electronic effects imparted by the environment on the regio- and stereoselectivity, the calculations are done in the gas phase as well as under the influences of NH- - -S hydrogen bonding and external electric field, following a preliminary study.[24]

Earlier theoretical studies on the hydroxylation mechanism of methane and ethane[24−29] and on the epoxidation mechanism of ethene by Cpd I,[30−32] revealed a two-state reactivity (TSR) scenario,[33] which originates in the closely lying triradicaloid states of Cpd I: a high-spin (HS) quartet state and a low-spin (LS) doublet state. It was found that on the HS surface the reactions proceed in a stepwise manner, whereas on the LS surface the reaction is effectively concerted. In addition the epoxidation mechanism[30] revealed a multistate scenario of the reaction intermediates, with iron in either oxidation state Fe^{III} or Fe^{IV} and in LS or HS situations. An interesting dilemma was already posed by these studies, which revealed a small barrier (14 kcal/mol) for epoxidation and a much larger one, >20 kcal/mol, for C−H hydroxylation.[27,29] With these disparate barriers, one wonders how can C−H hydroxylation ever become competitive with C═C epoxidation. Is this an intrinsic property of the substrate undergoing oxidation? Is it a result of electric field, hydrogen bonding, or both inside the protein pocket? Our preliminary results[26,34,35] indicated that Cpd I is a chameleon species that changes its character, depending on external interactions, such as those that are imparted in the protein pocket, and that these interactions have a major impact on the ordering of the hydroxylation vis-à-vis epoxidation transition states.[24] The present report addresses all these issues regarding the electronic factors that determine the C═C/C−H ratio and the stereoselectivity of both processes. In addition, we present a valence bond (VB) model that accounts for the electronic structure of the transition state of oxygenation by Cpd I and for the chameleonic behavior of Cpd I under external perturbation such as NH- - -S hydrogen bonding and electric field.

2. Methods

All methods used here were similar to those in our previous published studies and will be briefly summarized. The systems were modeled using the hybrid density functional B3LYP[36] combined with an LACVP basis set[37] on iron and a 6-31G basis set on the remaining atoms (hence, B3LYP/LACVP). Single-point calculations were done with higher basis sets, which include polarization and diffuse functions on all non-hydrogen atoms (hence B3LYP/LACVP+*). Since no large differences were noted between the B3LYP/LACVP and B3LYP/LACVP+* results, all additional calculations were carried out only with B3LYP/LACVP. All calculations were performed using the Jaguar 4.1[38] and Gaussian 98[39] program packages. The study generated many data (spin densities, charge distributions, detailed geometries, potential energy scans, etc.), which are useful but cannot be included here for space economy. In addition, since Jaguar and Gaussian give slightly different energies (±0.2 kcal/mol), much of the data exist in two sets and are therefore summarized in the Supporting Information.

Cpd I (Scheme 1, **b**), was modeled as an iron−oxo porphine complex, where the proximal thiolate ligand was truncated to SH. This was established as a sufficient model in previous studies.[27] The effect of hydrogen bonding to the sulfur ligand was mimicked by adding two

(23) Groves, J. T.; Avaria-Neisser, G. E.; Fish, K. M.; Imachi, M.; Kuczkowski, R. L. *J. Am. Chem. Soc.* **1986**, *108*, 3837.
(24) de Visser, S. P.; Ogliaro, F.; Sharma, P. K.; Shaik, S. *Angew. Chem., Int. Ed.* **2002**, *41*, 1947−1951.
(25) Harris, N.; Cohen, S.; Filatov, M.; Ogliaro, F.; Shaik, S. *Angew. Chem., Int. Ed.* **2000**, *39*, 2003.
(26) Ogliaro, F.; Cohen, S.; Filatov. M.; Harris, N.; Shaik, S. *Angew. Chem., Int. Ed.* **2000**, *39*, 3851.
(27) Ogliaro, F.; Harris, N.; Cohen, S.; Filatov, M.; de Visser, S. P.; Shaik, S. *J. Am. Chem. Soc.* **2000**, *122*, 8977−8989.
(28) Ogliaro, F.; Filatov, M.; Shaik, S. *Eur. J. Inorg. Chem.* **2000**, 2455.
(29) Yoshizawa, K.; Kamachi, T.; Shiota, Y. *J. Am. Chem. Soc.* **2001**, *123*, 9806−9816.
(30) de Visser, S. P.; Ogliaro, F.; Harris, N.; Shaik, S. *J. Am. Chem. Soc.* **2001**, *123*, 3037−3047.
(31) de Visser, S. P.; Ogliaro, F.; Shaik, S. *Angew. Chem., Int. Ed.* **2001**, *40*, 2871−2874.
(32) de Visser, S. P.; Ogliaro, F.; Shaik, S. *Chem. Commun.* **2001**, 2322−2323.
(33) (a) Shaik, S.; Filatov, M.; Schröder, D.; Schwarz, H. *Chem. Eur. J.* **1998**, *4*, 193. (b) Schröder, D.; Shaik, S.; Schwarz, H. *Acc. Chem. Res.* **2000**, *33*, 139.
(34) (a) Ogliaro, F.; Cohen, S.; de Visser, S. P.; Shaik, S. *J. Am. Chem. Soc.* **2000**, *122*, 12892−12893. (b) Ogliaro, F.; de Visser, S. P.; Cohen, S.; Kaneti, J.; Shaik, S. *ChemBioChem* **2001**, *2*, 848−851. (c) Ogliaro, F.; de Visser, S. P.; Groves, J. T.; Shaik, S. *Angew. Chem., Int. Ed.* **2001**, *40*, 2874−2878.
(35) For a recent review on Cpd I, see: Harris, D. L. *Curr. Opin. Chem. Biol.* **2001**, *5*, 724.
(36) (a) Becke, A. D. *J. Chem. Phys.* **1992**, *96*, 2155. (b) Becke, A. D. *J. Chem. Phys.* **1992**, *97*, 9173. (c) Becke, A. D. *J. Chem. Phys.* **1993**, *98*, 5648. (d) Lee, C.; Yang, W.; Parr, R. G. *Phys. Rev. B* **1988**, *37*, 785.
(37) (a) Hay, J. P.; Wadt, W. R. *J. Chem. Phys.* **1985**, *82*, 99. (b) Friesner, R. A.; Murphy, R. B.; Beachy, M. D.; Ringlanda, M. N.; Pollard, W. T.; Dunietz, B. D.; Cao, Y. X. *J. Phys. Chem. A* **1999**, *103*, 1913.
(38) *Jaguar 4.1*; Schrödinger, Inc.: Portland, Oregon, 2000.
(39) Frisch, M. J.; Trucks, G. W.; Schlegel, H. B.; Scuseria, G. E.; Robb, M. A.; Cheeseman, J. R.; Zakrzewski, V. G.; Montgomery, J. A., Jr.; Stratmann, R. E.; Burant, J. C.; Dapprich, S.; Millam, J. M.; Daniels, A. D.; Kudin, K. N.; Strain, M. C.; Farkas, O.; Tomasi, J.; Barone, V.; Cossi, M.; Cammi, R.; Mennucci, B.; Pomelli, C.; Adamo, C.; Clifford, S.; Ochterski, J.; Petersson, G. A.; Ayala, P. Y.; Cui, Q.; Morokuma, K.; Malick, D. K.; Rabuck, A. D.; Raghavachari, K.; Foresman, J. B.; Cioslowski, J.; Ortiz, J. V.; Stefanov, B. B.; Liu, G.; Liashenko, A.; Piskorz, P.; Komaromi, I.; Gomperts, R.; Martin, R. L.; Fox, D. J.; Keith, T.; Al-Laham, M. A.; Peng, C. Y.; Nanayakkara, A.; Gonzalez, C.; Challacombe, M.; Gill, P. M. W.; Johnson, B. G.; Chen, W.; Wong, M. W.; Andres, J. L.; Head-Gordon, M.; Replogle, E. S.; Pople, J. A. *Gaussian 98*; Gaussian, Inc.: Pittsburgh, PA, 1998.

Scheme 2. General Mechanistic Features Found in the Theoretical Study and Labels of the Corresponding Species

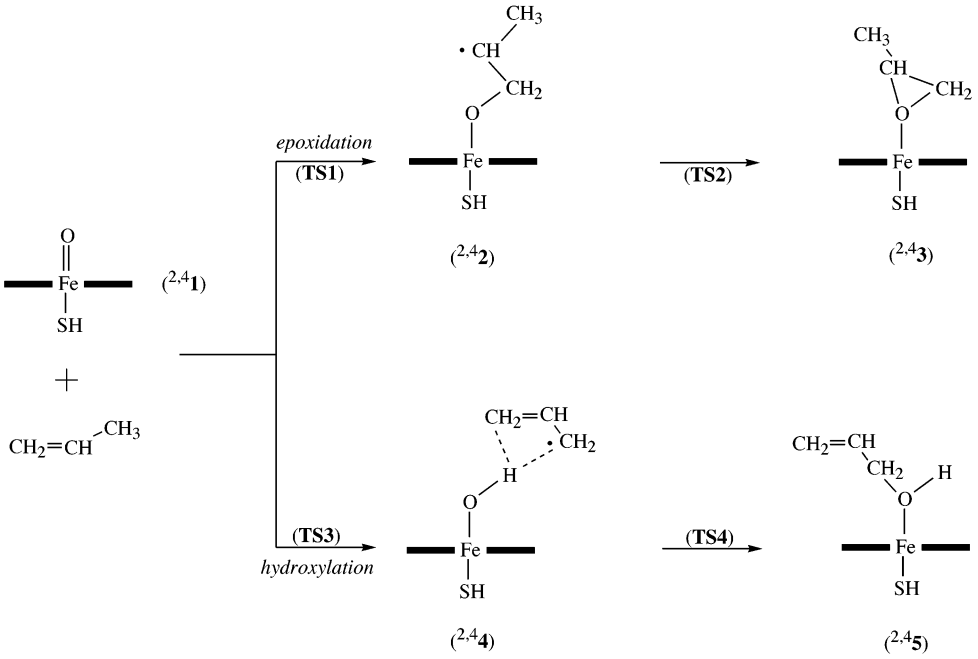

ammonia molecules to the system which point toward the sulfur of the proximal ligand at fixed distances of $r_{S\cdots HN} = 2.660$ Å.[24,34] The effect of polarization by the electric field was studied using the efficient continuum solvent model implemented in Jaguar 4.1 with a dielectric constant of $\epsilon = 5.7$ (and probe radius 2.72 Å). A recent, QM/MM study[40] in collaboration with the Mülheim group shows that the simple models represent the state of Cpd I in the protein pocket quite well.

Full optimization of all structures was carried out with the fast Jaguar 4.1 program package. Initially, geometry scans were generated in which one variable served as the "coordinate", while all the remaining degrees of freedom were fully optimized. The geometry scans were used as a starting point for the transition state searches. Since intrinsic reaction coordinate calculations for these large systems were computationally prohibitive, the scans were used to connect the transition states with the local minima and vice versa. All the scans are included in the Supporting Information as Figures S.1−S.7. Subsequently, all transition states and intermediates were characterized by frequency calculations. These calculations were done with Gaussian 98 that computes analytical frequencies, which are computationally less time-consuming and are more accurate than the routine implemented in Jaguar 4.1. All transition states mentioned hereafter had one imaginary frequency each. Single-point energy calculations on the optimized structures were employed to obtain the effects of NH- - -S hydrogen bonding and solvation by a dielectric medium. In our experience, the solvent calculations with Jaguar 4.1 occasionally give different solvation energies of two separate molecules and their supermolecule at a large intermolecular distance (of 10 Å). We therefore did not calculate absolute barriers relative to the separate reactants with $\epsilon = 5.7$ and preferred to compare relative transition-state energies.

The KIE of the hydroxylation reaction was studied using various models.[28,41] The Eyring model is based on eq 1 for the reaction rate constant k_r as a function of temperature T, the free energy of activation ($\Delta G^{\ddagger}$), the gas constant (R), and the frequency (A) of passing through the transition state (given by RT/Nh, N being Avogadro's number and h Planck's constant).

$$k_r = A \exp(-\Delta G^{\ddagger}/RT) \quad (1)$$

On the basis of this equation, the semiclassical KIE becomes, eq 2.

$$k_H/k_D = \exp[(\Delta G^{\ddagger}_D - \Delta G^{\ddagger}_H)/RT] \quad (2)$$

Corrections to the semiclassical KIE can be achieved by multiplying the Eyring KIE with the tunneling ratio ($Q_{t,H}/Q_{t,D}$) whereby Q_t is estimated from the Wigner correction in eq 3.[41]

$$Q_t = 1 + u_t^2/24 \quad \text{with} \quad u_t = h\nu/k_B T \quad (3)$$

Here, h is Planck's constant, k_B is the Boltzmann constant. and ν is the value of the imaginary frequency in the transition state. As in our study of methane hydroxylation,[28] here too the tunneling correction models due to Bell and Eckart were judged to be less suitable, mainly since they led to unrealistically large KIE values. The results obtained using the latter two tunneling models can be found in the Supporting Information.

3. Results

The Results section is divided into several parts. The first part summarizes the relevant molecular orbitals and their filling during the reaction process. The second part outlines the possible reaction pathways and electronic states leading to epoxidation products. The last part describes the corresponding hydroxylation pathways.

Scheme 2 summarizes some key species found in the study, starting with Cpd I in the $^{2,4}A_{2u}$ ground state (^{2,4}**1**). These features are similar to those in previous theoretical studies.[27,30] Propene can attack the oxo group of Cpd I with the terminal carbon atom of the olefin or with an allylic hydrogen. The former reaction will lead to C−O bond formation and radical complexes (^{2,4}**2**), which in a subsequent C−O bond formation step, lead to ring-closure of the epoxide ring and the formation of the epoxide−product complexes (^{2,4}**3**). The hydroxylation process starts with a hydrogen-atom transfer from propene to the oxygen of Cpd I, leading to the radical complexes, designated ^{2,4}**4**. Rebound of either one of the CH_2 groups onto

(40) Schöneboom, J. C.; Reuter, N.; Lin, H.; Thiel, W.; Cohen, S.; Ogliaro, F.; Shaik, S. *J. Am. Chem. Soc.* **2002**, *124*, 8142−8151.
(41) Melander, L.; Saunders, W. H., Jr. In *Reaction Rates of Isotopic Molecules*; Robert E. Krieger Publishing Company: Malabar, Florida, 1987.

Scheme 3. High-Lying Occupied Orbitals and Low-Lying Virtual Orbitals of Cpd I

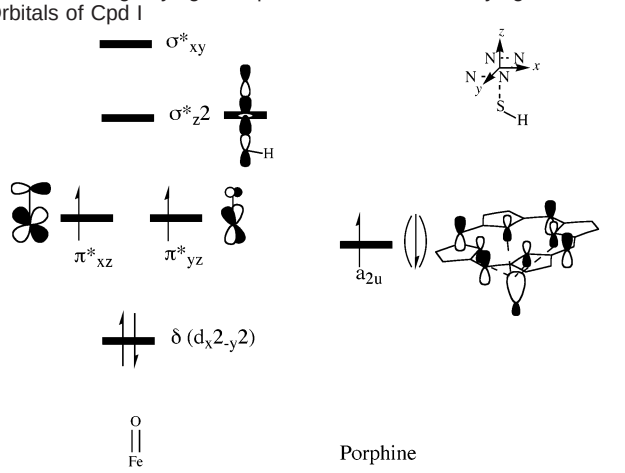

the oxygen atom gives the allyl alcohol product complex, ^{2,4}**5**. These mechanistic findings, with the exception of the TSR scenario, follow the rebound mechanism.[1−7,14,42,43] The hydroxylation products with and without allylic rearrangement are identical, but the different processes can nevertheless be traced by following the collapse of **4** to **5**. The transition states leading from ^{2,4}**1** to ^{2,4}**2** are designated ^{2,4}**TS1**, whereas the epoxide ring-closure transition states are designated as **TS2**. The hydrogen-transfer transition states in the hydroxylation step are designated ^{2,4}**TS3**, and the rebound transition states, **TS4**. All reaction processes presented here were studied in the doublet and quartet spin states. Furthermore, reaction paths via the two possible iron oxidation states (Fe^{III} and Fe^{IV}) were investigated.

3.1. Key Molecular Orbitals and Their Occupation during Epoxidation and Hydroxylation. The high-lying occupied and low-lying virtual orbitals of Cpd I are schematically depicted in Scheme 3. The left-hand-side shows the five d-block orbitals centered on the iron−oxo moiety, which are the $\delta(d_{x^2-y^2})$, π^*_{xz} and π^*_{yz}, $\sigma^*_{z^2}$ and σ^*_{xy}. The $\delta(d_{x^2-y^2})$ orbital is a nonbonding orbital made solely from the $d_{x^2-y^2}$ atomic orbital of iron, and is doubly occupied for all systems studied here. The π^*_{xz} and π^*_{yz} orbitals are antibonding in the Fe−O moiety. The π^*_{yz} orbital is slightly higher in energy than the π^*_{xz} orbital due to the additional antibonding interaction of the d_{yz} orbital on iron with the p_y orbital on sulfur. As a result of this, in the case of unevenly filled π^* orbitals, it is the π^*_{xz} orbital that will always have higher occupation (see later for the Fe^{III} states that have a $\delta^2\ \pi^*_{xz}{}^2\ \pi^*_{yz}{}^1$ configuration). The two highest-lying orbitals of the metal d-block of Cpd I are the σ^*_{xy} and $\sigma^*_{z^2}$, which are antibonding orbitals in the Fe−N linkages and the S−Fe−O linkages, respectively. The σ^*_{xy} orbital was empty in all systems described herein, while the $\sigma^*_{z^2}$ orbital becomes singly occupied in the two high-spin product complexes ^{4}**3** and ^{4}**5** (Scheme 2).

On the right-hand side of Scheme 3 we depicted the porphyrin-based orbital, which in D_{4h} symmetry is a_{2u}. The a_{2u} orbital mixes somewhat with the σ_S orbital on the sulfur ligand, and the amount of mixing depends on, among other things, the electric field and NH- - -S hydrogen bonding in the protein pocket.[34] The ground state of Cpd I is composed of two closely lying electronic states $^2A_{2u}$ and $^4A_{2u}$ that possess three unpaired

Scheme 4. Formal Electron Shifts from Propene toward Cpd I and the Corresponding Orbital Occupation in the Various Intermediates (**2** and **4**)

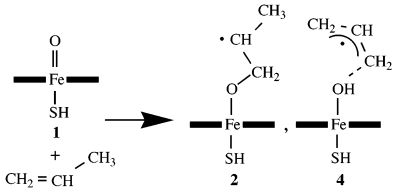

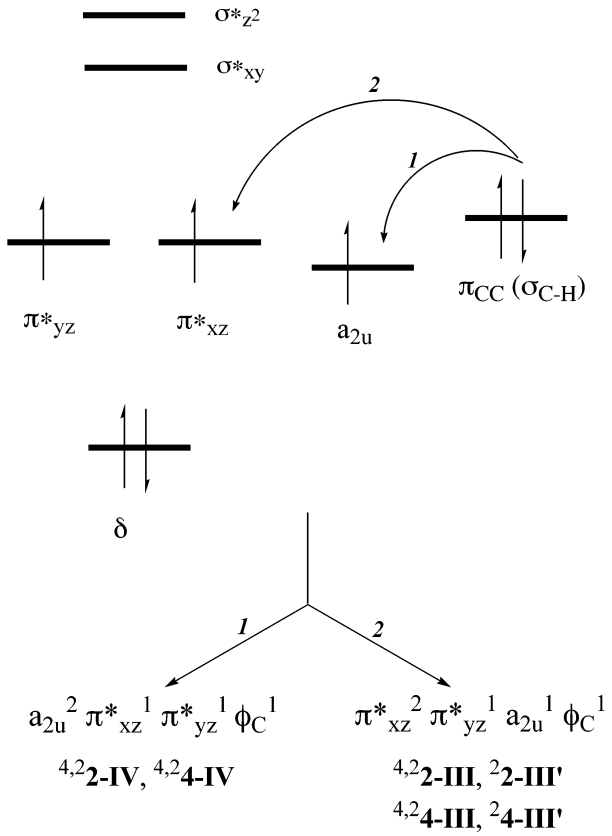

electrons in the π^*_{xz}, π^*_{yz} and a_{2u} orbitals. In both cases the two π^* orbitals contain an α-spin electron, while the a_{2u} orbital has α-spin in the $^4A_{2u}$ state and β-spin in the $^2A_{2u}$ state. Thus, formally, one counts the oxidation state of iron in Cpd I as Fe^V, although it is a combination of the d^4 configuration on iron, that is, Fe^{IV}, and the radical cation situation on porphyrin.

To keep track of the electron count during the transformation, we use the oxidation-state formalism, which assigns octet to all the ligands by taking electrons from the metal. The actual charges are smaller than those implied by the oxidation state, but the formalism gives a correct d-electron count of the metal in the complex. This formal electron count works in much the same way in epoxidation and hydroxylation mechanism, as illustrated in Schemes 4 and 5. The total process involves two "oxidation equivalents", in which the high-valent iron is transformed from formally Fe^V in Cpd I to formally Fe^{III} in the product complexes.

Scheme 5. Orbital Diagrams Describing the Occupation of the Product Complexes, ^{4,2}**3** and ^{4,2}**5**

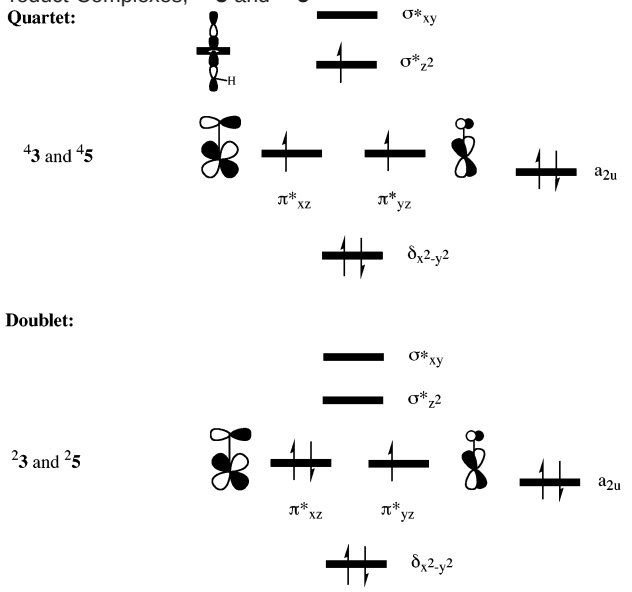

The first step of the reaction, in Scheme 4, which involves either O−C (epoxidation) or O−H (in hydroxylation) bond making, is attended by one electron shift from propene's $\pi_{C=C}$ or σ_{C-H} orbitals to one of the singly occupied MOs of Cpd I, and the propene orbital is converted to a localized ϕ_C orbital on either the CH or CH_2 moieties. A shift into the a_{2u} orbital leads to a $\pi^*_{xz}{}^1\ \pi^*_{yz}{}^1\ \phi_C{}^1$ configuration of the intermediate complexes ^{2,4}**2-IV** and ^{2,4}**4-IV**, whereby the iron retains the d^4 configuration and its oxidation state Fe^{IV}. The two unpaired electrons on iron have the same spin, while the third electron on a propene orbital (ϕ_C) has either the same spin, leading to the high-spin (HS) situation, or an opposite spin leading to the low-spin (LS) situation.

Alternatively, the electron can shift into the π^*_{xz} orbital, leading to a d^5 configuration on iron and an Fe^{III} oxidation state corresponding to the ^{2,4}**2-III** and ^{2,4}**4-III** intermediate complexes. These complexes have singly occupied π^*_{yz}, a_{2u}, and ϕ_C orbitals, and HS and LS states. In the LS situation the spins of the π^*_{yz} and a_{2u} electrons are singlet-paired, while ϕ_C has an α spin. Another pair of LS intermediates, labeled with a prime: ^{2}**2-III′** or ^{2}**4-III′**, pairs the electrons into a triplet pair in π^*_{yz} and a_{2u} electrons, while the ϕ_C orbital has a β-spin electron.

The second "oxidation equivalent" manifests during the conversion of the intermediates to the product complexes, by shifting the electron of ϕ_C into the iron π^*_{xz} orbital, in ^{2}**2-IV** and ^{2}**4-IV**, or into the a_{2u} orbital, in ^{2}**2-III** and ^{2}**4-III**. In each case, generation of the HS products will require an excitation of one electron into the $\sigma^*_{z^2}$ orbital of ^{4}**2-IV** or ^{4}**2-III**.[27] The product complexes are shown in Scheme 5. The HS complexes (^{4}**3** and ^{4}**5**) have a $\pi^*_{xz}{}^1\ \pi^*_{yz}{}^1\ \sigma^*_{z^2}{}^1$ configuration, whereas the low-spin complexes have only one singly occupied orbital, namely the π^*_{yz}. Hence, all product complexes contain iron d^5 configuration in the formal oxidation state Fe^{III}.

3.2. Epoxidation Mechanism. Previous work on the epoxidation of ethene by P450 showed[32] that a concerted synchronous oxygen insertion has a high-energy transition structure, with two imaginary modes, one of which converts the synchronous structure to the nonsynchronous transition state that lies 7.2 kcal/mol lower in energy. Therefore, the epoxidation process with propene was followed only for the nonsynchronous mechanism. Initially, the O- - -C bond formation can involve either the terminal CH_2 group or the central CH group. However, since the latter will give rise to a primary radical, which is less stable than a secondary radical, we restricted the study to the terminal CH_2 attack.

The epoxidation was found to have two distinct phases. First is the bond activation phase, in which the terminal carbon atom of the double bond attacks the oxygen atom of the iron−oxo species to form a C−O bond with the primary carbon and a radical center on the secondary carbon position. In a subsequent phase, called rebound, the epoxide ring is closed by an attack of the radical center on the oxygen atom. Relative energies of all calculated species are depicted in Figure 1. All energies are calculated relative to isolated propene and Cpd I in the $^4A_{2u}$ state (^{4}**1**). Single-point calculations with the LAVCP+* basis set, shown in parentheses, make the overall process more exothermic by ca. 12 kcal/mol but otherwise give very close results to the smaller basis set, LAVCP. Hereafter, we focus on the latter set of results only.

The C═C Bond Activation Phase. Starting from Cpd I in the $^4A_{2u}$ and $^2A_{2u}$ states (^{4,2}**1**) on the left-hand-side of Figure 1, the radical complexes (^{2,4}**2**) can be reached via a transition state (^{2,4}**TS1**). The bond-activation barriers are 10.0 (11.6) and 10.6 (12.4) kcal mol^{-1}, respectively, and pass via two low-lying transition states, indicated as ^{4}**TS1** and ^{2}**TS1**. The oxidation state on the iron is not indicated for these transition states, since they possess mixed oxidation states of the **III** and **IV** varieties. These transition states resemble the ones located in the study of ethene epoxidation.[30]

A few higher-lying transition states, labeled as ^{2,4}**TS1-III** and ^{2}**TS1-III′**, are indicated in the figure to correlate to the corresponding ^{2,4}**2-III** and ^{2}**2-III′** intermediates. The ^{4}**TS1-III** species could not be fully characterized as a transition state, since it invariably dropped to the lower-lying and more favorable ^{4}**TS1** state during the optimization. From our geometry scan (Figure S1), however, in which we managed to stay on the Fe^{III} potential energy surface, we could estimate a barrier of approximately 15.7 kcal mol^{-1}, see Supporting Information. The species ^{2}**TS1-III′** is found to be 20.5 kcal mol^{-1} higher in energy than the isolated reactants. As in the case of ethene epoxidation,[30] here too this structure originates from the excited state of Cpd I in which the π^*_{xz} and π^*_{yz} electrons are singlet paired and FeO is truly a doubly bonded Fe═O moiety. The geometry scan leading to this transition state was performed by extending the C−O bond distance starting from ^{2}**2-III′** in the direction of reactants. From the maximum energy along the scan a full geometry optimization was performed, leading to ^{2}**TS1-III′**. Although Figure 1 connects this transition state with ^{2}**2-III′**, the geometry of ^{2}**TS1-III′** indicates that it describes a concerted oxygen insertion (OCC angle of 79° in Figure 2). The intermediate state ^{2}**2-III′** itself is a shoulder that leads in a barrierless fashion to the product complex, ^{2}**3**. Indeed, frequency analysis of ^{2}**TS1-III′** featured two imaginary frequencies (see Figure 2). The one corresponding to frequency of i674.7 cm^{-1} is the concerted vibrational mode representing a simultaneous bond formation. A second mode with frequency of i139.5 cm^{-1} represents a cartwheel rotation that leads to the lower nonsynchronous transition state, ^{2}**TS1**, much like in our previous study of ethene epoxidation.[32]

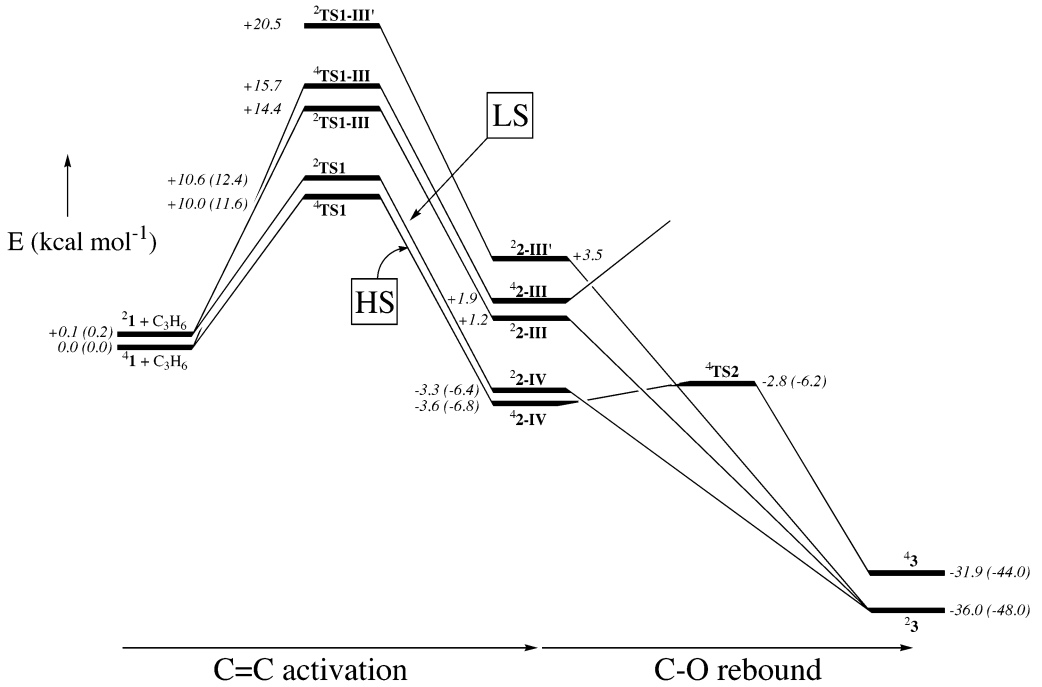

Figure 1. Reaction profiles for propene epoxidation by Cpd I. Values in parentheses are single-point B3LYP/LACVP+* results, while all values without parentheses are B3LYP/LACVP results (Jaguar 4.1 energies are used).

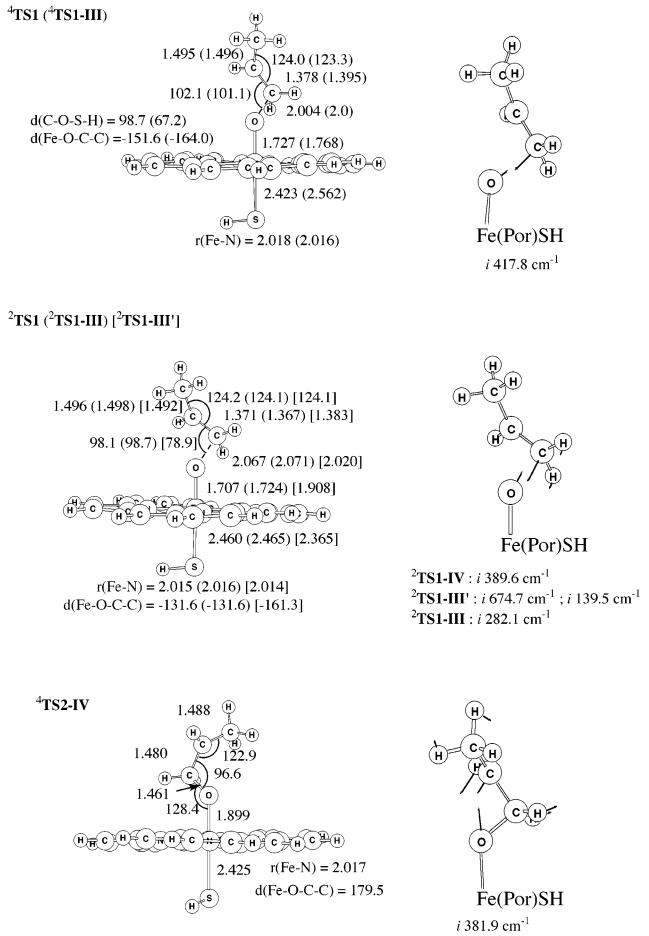

Figure 2. Transition-state structures and corresponding imaginary modes for the epoxidation mechanism.

Finally, although we correlated the **TS1-III** species to **2-III**, this does not mean that these intermediates are not dynamically accessible from the low-lying transition-state species, ^{4,2}**TS1**, which can lead to all the possible intermediate species, of the **2-IV** and **2-III** varieties.

The C- - -O Rebound Phase. The results of the scans for the ring-closure step starting from the five radical complexes ^{4,2}**2-IV**, ^{4,2}**2-III**, and ^{2}**2-III′** are depicted in Figure S.2 in the Supporting Information. These scans form the basis for the description of the rebound phase in Figure 1 here. All the scans starting from the LS intermediates, ^{2}**2-IV(III, III′)**, were found to lead in a barrierless ring closure to the product complexes ^{2}**3**, in agreement with the corresponding results for ethene epoxidation.[30] However, the HS intermediates feature barriers for rebound. A rebound transition state (^{4}**TS2** in Figure 1) with a barrier of 0.8 (0.6) kcal mol^{-1} was located for the conversion of ^{4}**2-IV** to ^{4}**3**. This barrier is lower than the one found along the rebound path of ethene epoxidation of 2.3 kcal mol^{-1}.[30] Along the scan starting from ^{4}**2-III**, we could not localize the transition state, and the scan shows that the rebound barrier for the ring closure from ^{4}**2-III** to ^{4}**3** is at least larger than 9 kcal mol^{-1}, compared with 7.2 kcal mol^{-1} in ethene epoxidation.[30]

Geometries. Optimized geometries of all transition states (**TS1** and **TS2**) are depicted in Figure 2 along with the imaginary modes for the lowest species, ^{2,4}**TS1** and ^{4}**TS2**. The optimized intermediate complexes and product complexes are depicted in Figure 3.

The main differences, in Figure 2, are seen in the Fe−O and Fe−S bond lengths of the Fe^{III} and Fe^{IV} species. In the Fe^{III} states, the π^*_{xz} orbital is doubly occupied, and since this orbital involves antibonding interaction in the Fe−O moiety, this results in elongation of the Fe−O bond lengths in the Fe^{III} states. Most geometries are quite similar to the ones obtained in the reaction of ethene with Cpd I,[30] and the lower activation barriers in the propene case are reflected in the less activated geometries of the double bond and the Fe−S and Fe−O distances for the propene case (e.g., compare ^{4}**TS1** to ^{4}**TS1**(CH_2═CH_2) in ref

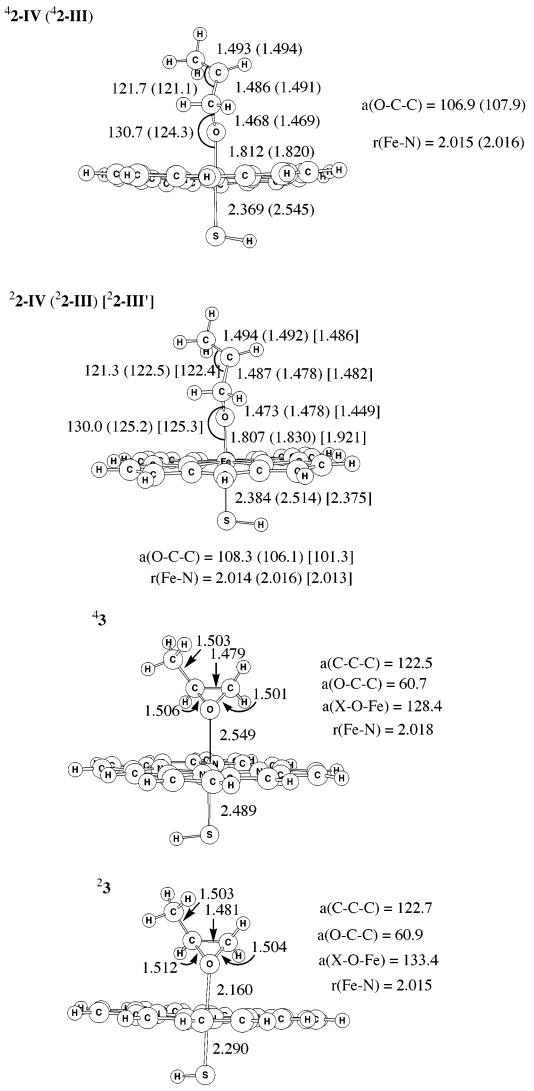

Figure 3. Structures of the intermediate and product complexes for the epoxidation mechanism.

30, where the C═C distance is 1.396 Å, the Fe−O distance is 1.743 Å, and the O−C distance is advanced, 1.893 Å).

Much the same as with ethene,[30] here too the propene moiety in ^{2,4}**TS1** extends upright (dihedral angle FeOCC is ca. 132° and 152°, respectively) to avoid steric repulsions with the porphyrin. In the enzyme pocket, this extension may not be possible due to steric constraints. A parallel orientation of the alkenyl moiety (making the dihedral angle FeOCC ca. 90°) may then be enforced,[32] thus differentiating between *cis*- and *trans*-alkenes due to steric repulsion between one of the trans substituents and the porphyrin macrocycle.[1a] The intermediates ^{2,4}**2-IV** retain the extended conformation, much like that in the ethene study.[30]

The product complexes, ^{2,4}**3**, in Figure 3 exhibit a difference compared with ethylene oxide.[31] Thus, while in the ethylene case, the epoxide was oriented perpendicular to the porphyrin ring, here with propene as a substrate, the epoxide ring is tilted; the angle formed by the epoxide plane and the Fe−O bond is 128−133°. This may be due to the formation of a weak hydrogen bond between the hydrogen of the epoxide with a nitrogen atom from the porphyrin ring. This structure of the product complex is akin to the complex identified by Groves et al.[44] en route to alkene epoxidation by a ruthenium−oxo porphyrin catalyst.

3.3. Hydroxylation Mechanisms. In principle, the hydrogen abstraction from propene could have taken place from any of the three carbon atoms. G2/6-311++G**//B3LYP/6-311++G** calculations on the three possible hydrogen-abstraction reactions show that the most stable radical is allyl, with a bond dissociation enthalpy (ΔH_r) of 88.7 kcal mol^{-1}. This is in perfect agreement with photoelectron spectroscopy measurements of Wenthold et al.[45] who obtained 88.8 ± 0.4 kcal mol^{-1}. Hydrogen abstraction from the C^1 and C^2 positions is calculated to be 22.2 and 24.4 kcal mol^{-1} more endothermic, respectively. Therefore, the study of the mechanism of hydroxylation of propene by Cpd I was restricted to the allylic hydroxylation.

The allylic hydroxylation of propene by Cpd I is shown in Figure 4. All energies are relative to isolated propene and Cpd I in the $^4A_{2u}$ state. The values in parentheses correspond to the LACVP^{+}* basis set. Again, the higher basis set makes the process more exothermic by 6−7 kcal/mol, but otherwise the barriers are similar to the smaller basis, which is used henceforth. The mechanism exhibits two phases. In the first phase, a hydrogen atom is transferred from the methyl group to the oxygen of the iron−oxo moiety. In a subsequent phase, the allyl radical reorients opposite to the OH bond, and either of its terminal carbons attacks the oxo group to form a C−O bond and a ferric−alcohol product complex. Five intermediate complexes ^{2,4}**4-IV**, ^{2,4}**4-III**, and ^{2}**4-III′** were located. The lowest one of these is the ^{2}**4-IV** species with the ^{4}**4-IV** state just 0.1 (0.4) kcal mol^{-1} higher. The intermediate states with the iron in oxidation state Fe^{III} are higher in energy.

C−H Activation Phase. The C−H activation occurs via the lower-lying transition states, indicated as ^{2,4}**TS3**, with barriers of 13.4 (15.8) and 13.7 (16.1) kcal mol^{-1}, much lower than the corresponding barriers computed for the hydroxylations of methane[27] and ethane.[29] Once again there is no indication of the iron's oxidation state in ^{2,4}**TS3** since these species possess a mixed oxidation state.

The higher-lying transition states with iron in the oxidation state Fe^{III} (^{2}**TS3-III** and ^{2}**TS3-III′**) could not be fully characterized, since they fell down to the lower-lying ^{2}**TS3** species. Their structures were estimated from the corresponding geometry scans, depicted in Figure S.3 in the Supporting Information. Both Fe^{III} hydrogen-transfer transition states are 14−15 kcal mol^{-1} higher in energy than the corresponding **TS1** transition states in Figure 4. Since the scans exhibit a spike-like behavior in the energy, the Fe^{III} barriers reported in Figure 4 may well be lower estimates. Very likely, the HS Fe^{III} transition state is of the same order of magnitude as well.

The C- - -O Rebound Phase. In the intermediates ^{2,4}**4-IV**, the allylic moiety is connected to iron hydroxo species via a weak FeOH- - -C hydrogen bond (see Figure 6 later). An extensive search to locate a transition state for the LS rebound

(42) (a) Groves, J. T. *J. Chem. Educ.* **1985**, *62*, 928−931. (b) Groves, J. T.; McClusky, G. A. *J. Am. Chem. Soc.* **1976**, *98*, 859−861. (c) Groves, J. T.; van der Puy, M. *J. Am. Chem. Soc.* **1976**, *98*, 5290−5297.
(43) Gelb, M. H.; Heimbrook, D. C.; Mälkönen, P.; Sligar, S. G. *Biochemistry* **1982**, *21*, 370.
(44) Groves, J. T.; Ahn, K.-W.; Quinn, R. *J. Am. Chem. Soc.* **1988**, *110*, 4217−4220.
(45) Wenthold, P. G.; Polak, M. L.; Lineberger, W. C. *J. Phys. Chem.* **1996**, *100*, 6920.

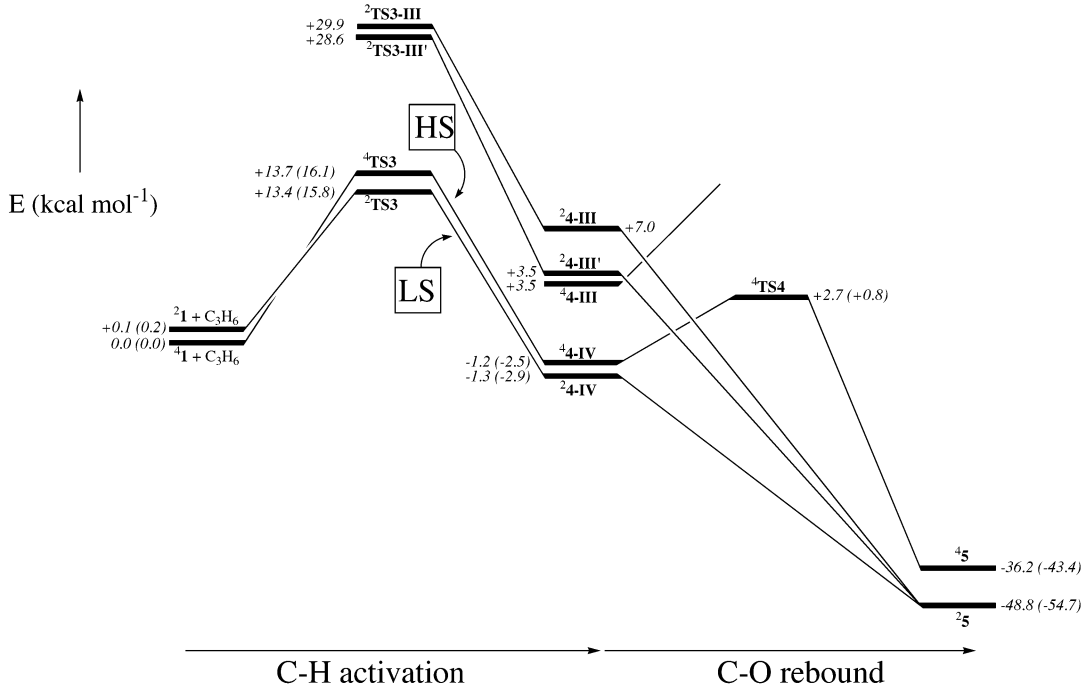

Figure 4. Reaction profiles for allylic hydroxylation of propene by Cpd I. Values in parentheses are single-point B3LYP/LACVP+* results, while all values without parentheses are B3LYP/LACVP results (Jaguar 4.1 energies are used).

was performed along several different scans. Using an OH rotation about the Fe−O bond as the scanning coordinate gave a relatively high-energy process and was abandoned for lower-energy paths. Using the Fe−O−H−C dihedral angle[29] as a scanning coordinate gave a species 2.4 kcal/mol higher than ^{2}**4-IV**, but its frequency analysis revealed three imaginary frequencies. The path along this mode was found to transform the FeOH- - -C hydrogen bond in ^{2}**4-IV** to the HC- - -O(H)Fe type, where a small reorientation of the C−H bond resulted in a steep energy descent toward the alcohol complex. Finally, using the C- - -O distance as the scanning coordinate resulted in a very shallow energy profile that rose to 1.5 kcal/mol above ^{2}**4-IV** and fell down to the product, ^{2}**5**. The top structure involves allyl rotation around the Fe−O bond, but is not a real rebound transition state. In a similar fashion, all the LS rebound processes were found to proceed in a barrierless fashion. Thus, the corresponding radical species on the LS manifold are more like shoulders with flat ridges on the potential energy surface rather than true intermediates. In contrast, using the same scan as in the LS case, the HS rebound process revealed a distinct transition state, ^{4}**TS4**, and had a significant barrier of 3.9 (3.3) kcal mol^{-1}. Figures S.4−S.6 in the Supporting Information show the scans of the rebound phase and demonstrate that *the rebound occurs by rotation of the allyl group about the Fe−O bond as the C- - O distance shortens.*

In principle, the rebound step in the hydroxylation can take place via an attack of C_α onto the oxygen atom or via an attack of C_γ onto the oxygen atom. We performed two geometry scans for the rebound process starting from ^{4}**4-IV** in which we investigated the two possible rebound mechanisms with variable C_α−O bond lengths and with variable C_γ−O bond lengths, respectively (see Figure S.7 in the Supporting Information). Both rebound processes were found to have a similar reaction barrier. Thus, the allyl radical in ^{4}**4-IV** is weakly bound and can easily lead to allylic rearrangement. However, since ^{4}**4-IV** has a barrierless rebound path, the allyl radical in this species will have a much shorter lifetime to rearrange.

Geometric Features in the Bond-Activation Phase. Optimized geometries of the hydrogen-transfer transition states (^{2,4}**TS3**) and rebound transition state (^{4}**TS4**) are plotted in Figure 5 along with the frequencies of the imaginary modes.

The imaginary frequencies of ^{4}**TS3** and ^{2}**TS3** are high and mark these species as hydrogen-transfer transition states. The important geometrical differences between ^{4}**TS3** and ^{2}**TS3** are the location of the hydrogen atom. In the LS situation, the hydrogen atom is closer to the carbon atom (r_{C-H} = 1.244 Å) than to the oxygen atom (r_{O-H} = 1.318 Å) and is, therefore, more reactant-like in character. On the contrary, the ^{4}**TS3** structure has a more product-like geometry with r_{C-H} = 1.337 Å and r_{O-H} = 1.257 Å. Nevertheless, both these transition states have the hydrogen in a rather central position between the carbon and oxygen atoms, and the angle of the C- - -H- - -O triad is virtually linear. In comparison, our earlier results on the hydroxylation of methane by Cpd I[27,28] showed the analogues of ^{4,2}**TS3** to be typified by very stretched C−H bonds (r_{C-H} = 1.500 Å for the HS process and r_{C-H} = 1.510 Å for the LS process), but the C- - -H- - -O angle was again almost linear. Indeed, the barriers for C−H hydroxylation in the two cases reflect the differences in C- -H extension in the transition states; in the hydroxylation of methane the barriers are 26.5 (LS) and 26.7 (HS) kcal mol^{-1} but only 13.4 (LS) and 13.7 (HS) kcal mol^{-1} for propene.

Geometric and Other Features in the Rebound Phase. All the intermediate complexes (^{2,4}**4**) and product complexes (^{2,4}**5**) are depicted in Figure 6. The intermediate complex (^{2,4}**4**) in the hydroxylation contains an allyl radical (CH_2−CH−CH_2•) coordinated to the iron−hydroxo species by weak FeOH- - -C hydrogen bonds. The two C−O distances in ^{4}**4-IV** are not equal, and the initial bond distance C_α−O is 3.490 Å, whereas C_γ−O is 4.139 Å. The weak binding of the radical to the iron−hydroxo

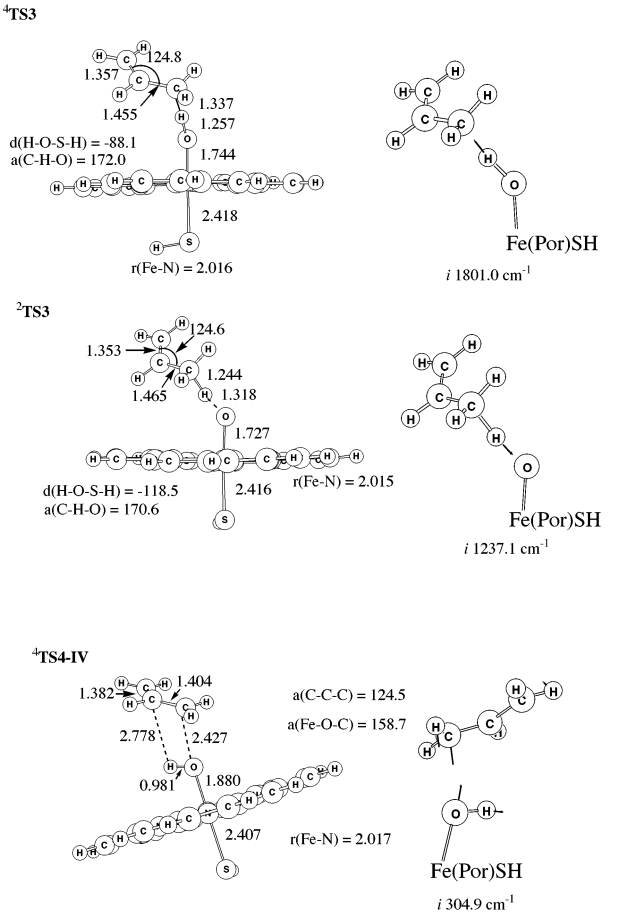

Figure 5. Transition-state structures and corresponding imaginary modes for the hydroxylation mechanism.

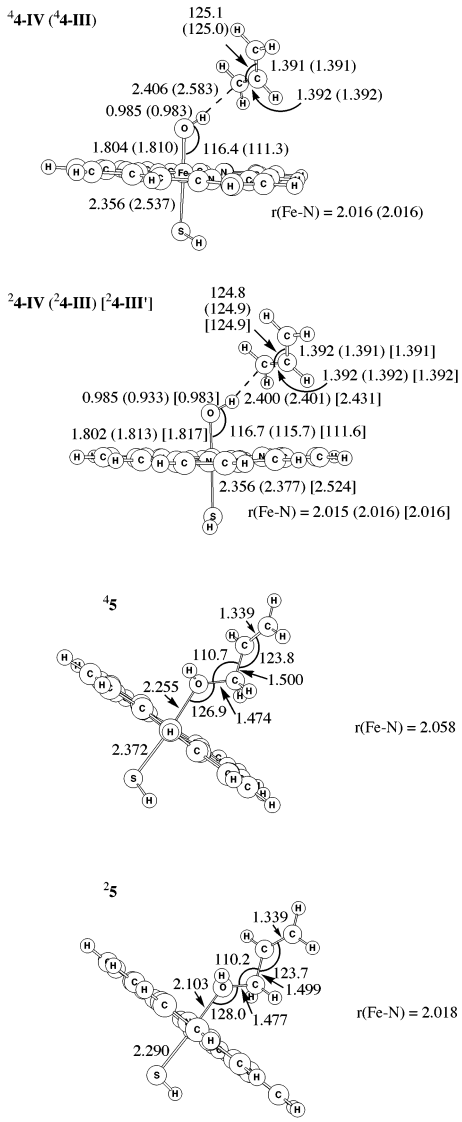

Figure 6. Structures of the intermediate and product complexes for the hydroxylation mechanism.

moiety is apparent from the fact that the spin density in the allylic moiety is distributed equally between the two terminal CH_2 groups and the central CH group has a negative spin density, as in a free allyl radical (See Table S1 in the Supporting Information, and Figure 10 later on).

Additional features, which show this weak binding of the allylic moiety to iron−hydroxo in the intermediates ^{2,4}**4-IV**, are the set of low-frequency modes ($\leq$95 cm^{-1}), which describe the relative motion of the allylic moiety with respect to the iron−hydroxo species. These modes are collected in the Supporting Information (Table S.15). One such low-frequency mode describes the allyl swing from C_α to C_γ and accounts for the ease of the allylic rearrangement during the rebound. Another set of modes (frequencies 12−35 cm^{-1}) describes the rotation of the allylic moiety about the Fe−O bond away from the FeOH- - -C hydrogen bond to the rebound position (C- - -O(H)-Fe interaction), beyond which the rebound takes place. Yet another mode with a somewhat higher frequency describes a flip of the allylic group that changes the plane, which is coordinated to the iron−hydroxo. This mode will account for inversion of the configuration (e.g., when the CH_3 group is made chiral by isotopic labels, i.e., CHDT). Thus, the radical has a great deal of freedom, but this freedom is not isotropic because certain modes are more restricted than others, and this restriction will become more apparent within the protein pocket that will allow allylic swing but restrict the allylic flip. This restricted freedom has been known ever since the study of bicyclo[2.1.0]-pentane by Ortiz de Montellano[46] revealed that the resulting radical can rearrange but rebounds only from the original face (i.e., restricted flip mode). Other evidence for a similar behavior has been reviewed[1a,4] and noted recently in the hydroxylation study of bicyclic probes by a few P450 isozymes, by Groves, Ortiz de Montellano, et al.[47]

These modes are common to both the HS and LS intermediates. However, in the LS intermediate, once the allyl rotates about the Fe−O bond to the rebound position (at a very low energy cost), the ensuing rebound process itself is barrierless, whereas in the HS intermediate the rebound process encounters a barrier. The rebound transition state ^{4}**TS4**, in Figure 5, has an Fe−S bond of 2.407 Å and an Fe−O bond of 1.880 Å. Both bonds are considerably longer than the corresponding ones in the ^{4}**4-IV** intermediate (Figure 6). This behavior is in agreement with the results obtained for methane hydroxylation,[25,27] and indicates that the HS rebound has a true chemical transition

(46) Ortiz de Montellano, P. R.; Stearns, R. A. *J. Am. Chem. Soc.* **1987**, *109*, 3415−3420.
(47) Auclair, K.; Hu, Z.; Little, D. M.; Ortiz de Montellano, P. R.; Groves, J. T. *J. Am. Chem. Soc.* **2002**, *124*, 6020−6027.

Table 1. Kinetic Isotope Effect on the Hydrogen Transfer Step in the Hydroxylation Mechanism via the ^{4}TS3 and ^{2}TS3 Transition States

label[a]	$\Delta G^{\ddagger}_{gas}$ (kcal mol^{-1})	imaginary frequency (cm^{-1})	k_H/k_D (Eyring)[b]	k_H/k_D (Wigner)[c]
		^{4}TS3		
all-h	21.2	i1801.0	-	-
3-d_1	22.3	i1356.6	6.6	9.7
2-d_1	21.2	i1800.9	1.0	1.0
1-d_1	21.2	i1800.9	1.0	1.0
3-d_3	22.4	i1339.7	7.0	10.5
All-d	22.4	i1339.4	7.0	10.5
		^{2}TS3:		
All-h	21.4	i1237.1	-	-
3-d_1	22.4	i1000.2	5.6	7.1
2-d_1	21.3	i1236.8	1.0	1.0
1-d_1	21.4	i1236.9	1.0	1.0
3-d_3	22.4	i976.0	5.9	7.7
All-d	22.4	i975.4	5.9	7.7

[a] The nomenclature is as follows: the first number represents the carbon atom, in $C^1H_2{=}C^2H{-}C^3H_3$, where the hydrogen is replaced by deuterium. The number of H→D replacements is the subscript to d. [b] Calculated using the semiclassical model of Eyring, eq 2. [c] Calculated using the tunneling approximation due to Wigner, eq 3.

state that requires Fe−S and Fe−O bond lengthening. The source of activation was ascribed[25,27] to the need to shift an electron from the alkyl moiety to the high lying $\sigma^*_{z^2}$ orbital (Scheme 5) to conserve the quartet-spin during the HS rebound process. Please note also that the Fe- - -O- - -C angle (ca. 159°) at the rebound transition state, **^{4}TS4**, is close to 180°, thus indicating that the allyl tries to maintain overlap with the $\sigma^*_{z^2}$ orbital that accepts the electron. In contrast, along the LS rebound path, where such an excitation is not required and the electron is shifted to the low-lying π^* orbital, the Fe−S bond shortens during rebound (from 2.356 to 2.290 Å). This Fe−S bond shortening mitigates the Fe−O lengthening and creates a barrierless process. Thus, the lifetime of the LS intermediate will be ultra-short and limited by the rotational mode that the allyl group has to perform to assume a rebound position.

H/D Kinetic Isotope Effects in C−H Hydroxylation. Hydroxylation reactions of Cpd I with alkanes are known to exhibit a large KIE.[1a,4,48−54] The KIE values for allylic hydroxylation of propene are presented in Table 1. Originally, the imaginary frequency in the **^{4}TS3** transition state is i1801 cm^{-1}. This value drops to i1356.6 cm^{-1} when a deuterium atom replaces the transferred hydrogen atom. Additional substitution of the other two hydrogen atoms attached to the allylic carbon atom (C^3) results in a further lowering of the imaginary frequency to i1339.7 cm^{-1}. The same effects are also visible in the KIE studies of the LS process via **^{2}TS3**. In this species, the replacement of the reactive hydrogen atom by a deuterium atom lowers the imaginary frequency from i1237.1 cm^{-1} to i1000.2 cm^{-1}. Substitution of all hydrogen atoms attached to the allylic carbon atom by deuterium atoms lowers the imaginary frequency to i976.0 cm^{-1}. H/D substitution away from the reaction center on C^1 and C^2 has a minor change on the imaginary frequency.

The significant lowering of the imaginary frequencies in **^{4,2}TS3** after deuterium substitution is in accord with the nature of these transition states as hydrogen-abstraction species. This assignment is supported by the linear O- - -H- - -C moiety (Figure 5) and the spin-density distribution.[28] In accord, the semiclassical primary KIE values are large, 6.6 (**^{4}TS3**) and 5.6 (**^{2}TS3**), and Wigner correction due to tunneling further raises these values to 9.7 (**^{4}TS3**) and 7.1 (**^{2}TS3**). These KIE values are similar to the ones we calculated[28] for the methane hydroxylation by Cpd I. Experimentally determined primary KIE values for the hydroxylation of toluene and *p*-xylene by P450 are, respectively, 5.9 ± 0.35 and 6.4 ± 0.9,[51] while for allylic hydroxylation KIE values of 8−12 were obtained.[1a,4] The secondary and tertiary KIE values are negligible, of the order of 1.0. In conclusion, the values computed in Table 1 are in good agreement with experimental values and with the contention that the transition states for the initial step of hydroxylation are essentially hydrogen-abstraction species.

Table 2. Relative Energies (without and with Zero-Point Corrections), Enthalpies (ΔH), and Free Energies (ΔG)[a]

cmpd	ΔE	$\Delta(E+\text{ZPE})$	$\Delta H^{298\,K}$	$\Delta G^{298\,K}$
^{4}**1**+C_3H_6	0.00	0.00	0.00	0.00
^{2}**1**+C_3H_6	0.06	0.03	0.08	0.37
		Epoxidation:		
^{4}**TS1**	9.71	10.29	9.98	22.38
^{4}**2-IV**	−3.89	−2.63	−2.12	7.62
^{4}**TS2−IV**	−2.99	−2.33	−1.95	7.95
^{4}**3**	−32.00	−29.89	−29.72	-19.54
^{2}**TS1**	10.42	10.61	10.67	21.97
^{2}**2-IV**	−3.43	−2.43	−2.34	8.74
^{2}**3**	−35.99	−32.57	−32.66	-20.08
		Hydroxylation:		
^{4}**TS3**	13.53	10.63	10.92	21.21
^{4}**4-IV**	−1.27	−2.38	−1.75	7.58
^{4}**TS4−IV**	2.38	1.04	1.79	11.11
^{4}**5**	−35.97	−34.11	−33.52	-24.05
^{2}**TS3**	13.52	10.83	11.28	21.35
^{2}**4-IV**	−1.60	−2.54	−1.38	6.40
^{2}**5**	−49.03	−45.83	−45.64	-34.21

[a] Data based on frequency calculation with Gaussian 98. All values are in kcal/mol.

Table 3. Environmental Effects on the Species Involved in the Rebound Phase

cmpd	ΔE[a]	$\Delta(E+\text{ZPE})$[b]	$\Delta E_{\epsilon=5.7}$[a]	$\Delta E_{2(\text{NH}\cdots\text{S})}$[a]
		Epoxidation:		
^{4}**2-IV**	0.00	0.00	0.00	0.00
^{4}**TS2**	0.90 [b]	0.30	0.59	2.55
^{4}**2-III**	5.48	-	5.41	-
^{2}**2-IV**	0.46 [b]	0.20	0.77	1.55
^{2}**2-III**	4.74	-	4.11	-
^{2}**2-III′**	7.02	-	4.86	-
		Hydroxylation:		
^{4}**4-IV**	0.00	0.00	0.00	0.00
^{4}**TS4**	3.65 [b]	3.42	5.17	2.47
^{4}**4-III**	4.40	-	2.14	-
^{2}**4-IV**	−0.33 [b]	−0.16	0.04	−0.49
^{2}**4-III**	7.91	-	2.79	-
^{2}**4-III′**	4.44	-	1.86	-

[a] All ΔE data are calculated with Jaguar 4.1, unless noted otherwise. [b] Calculated with Gaussian 98.

Data Concerning the Other Aspects of C=C Epoxidation and C−H Hydroxylation. Table 2 summarizes the effects of zero-point energies and other thermal factors on the energetic of both mechanisms. Table 3 shows relative energies in a dielectric medium with $\epsilon = 5.7$ and two external NH- - -S

(48) Groves, J. T.; Watanabe, Y. *J. Am. Chem. Soc.* **1986**, *108*, 507.
(49) Sorokin, A.; Robert, A.; Meunier, B. *J. Am. Chem. Soc.* **1993**, *115*, 7293.
(50) Atkinson, J. K.; Hollenberg, P. F.; Ingold, K. U.; Johnson, C. C.; Le Tadic, M. H.; Newcomb, M.; Putt, D. A. *Biochemistry* **1994**, *33*, 10630.
(51) Manchester, J. I.; Dinnocenzo, J. P.; Higgins, L. A.; Jones, J. P. *J. Am. Chem. Soc.* **1997**, *119*, 5069.

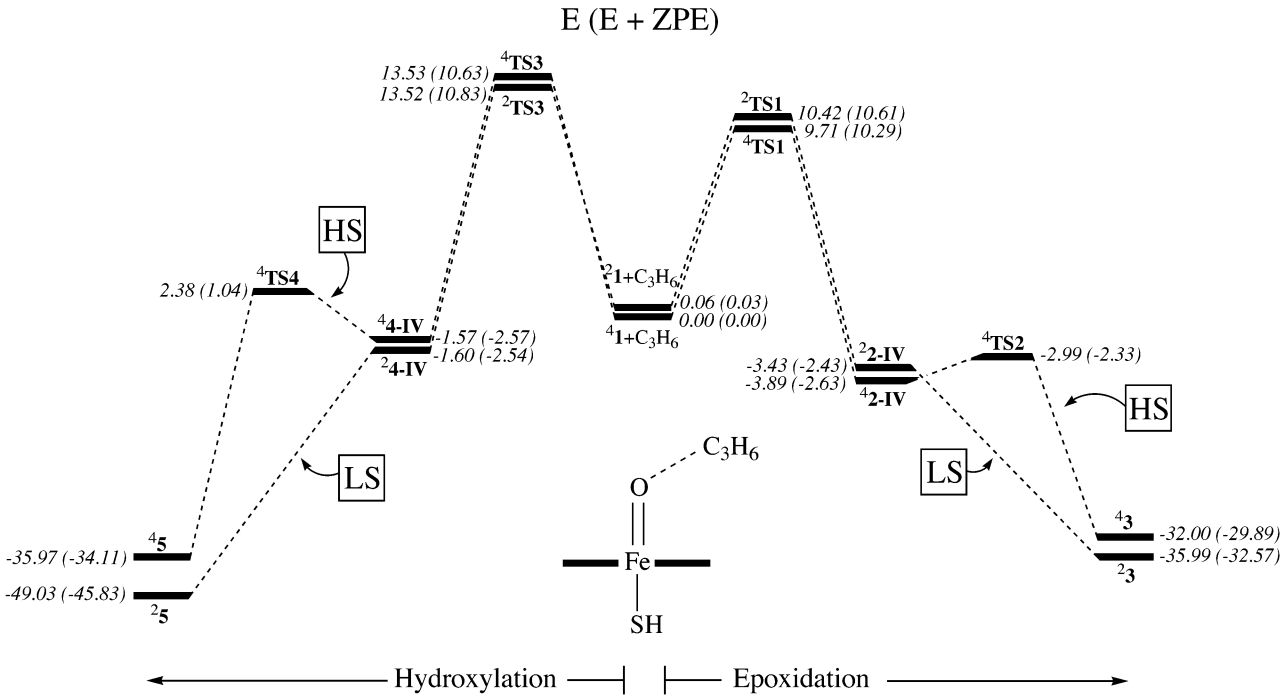

Figure 7. Gas-phase relative energies for the lowest-energy pathways of allylic hydroxylation and epoxidation of propene by Cpd I. Values out of parentheses are energy only (E), while values in parentheses include zero-point energies (E + ZPE). Gaussian 98 energies are used.

hydrogen bonds for the intermediates and rebound steps. These data will be used in the discussion.

4. Discussion

4.1. General Mechanistic Features. Figure 7 summarizes the low-energy pathways for the two mechanisms. The energetically favorable mechanisms occur along nonsynchronous bond activation (C═C or C−H) phases, leading to a carbon radical species, followed by a rebound phase that leads to C−O bonding. The LS pathways, however, are effectively concerted and the radical species in them, ^{2}**2-IV** and ^{2}**4-IV**, behave more like shoulders than true intermediates, collapsing to the product complexes in a virtually barrierless manner. In contrast, the HS paths proceed via genuine intermediates, ^{4}**2-IV** and ^{4}**4-IV**, that have barriers for C- - -O bond formation.

The hydroxylation rebound barrier (via ^{4}**TS4-IV**) is significant in the gas phase and gets larger with medium polarization effect included (5.2 kcal mol^{-1}, Table 3). This barrier endows the HS intermediate with sufficient lifetime to undergo stereochemical scrambling, especially allylic rearrangement by swinging the two allylic positions. Allylic rearrangement is well documented.[1a,4,13−15] Thus, for example, the hydroxylation of 3,3,6,6-tetradeuteriocyclohexene, methylenecyclohexane, and β-pinene with P450$_{LM2}$ by Groves and Subramanian[14] showed significant allylic rearrangement, which varied up to almost complete scrambling in some instances. Nevertheless, stereochemical scrambling is not always observed, as indicated by the results of Woggon et al.[53,54] in the study of geraniol and P450$_{cath}$, which led to complete stereo- and regiospecific hydroxylation. Our study does not account for this result that may originate either in properties of the geraniolyl radical (e.g., its donor ability which lowers the rebound barrier, as predicted in the study of methane hydroxylation[27]) or in steric constraints within the protein pocket, which may limit the freedom of the radical movements.

The rebound barrier in the epoxidation (via ^{4}**TS2**) is only 0.9 kcal mol^{-1}, and while it increases to 2.6 kcal/mol with NH- - -S hydrogen bonding (see Table 3), it nevertheless remains small. The small barrier will lead to a short lifetime of the intermediate, ^{4}**2-IV**, and consequently less stereochemical scrambling is expected in epoxidation. The study of Groves et al.[23] on the reactivity of *trans*-1-deuteriopropene with P450$_{LM2}$ resulted in *trans*-1-deuteriopropylene oxide. However, the observation of stereospecific H/D exchange in the presence of D_2O indicated the presence of an intermediate. It was proposed that this intermediate can either be a metallacycle or an *N*-alkyl heme precursor. Considering our present results and based on our study of suicide deactivation of the heme en route to epoxidation,[31] we suggest that an *N*-alkylated heme could result from the intermediates ^{4}**2-III**, which are longer-living than ^{4}**2-IV**. The peculiar H/D exchange, however, was limited to propene and was not observed for higher analogues.[23] Similarly, Vaz et al.[22] reported that the epoxidation of *cis*- and *trans*-butenes is completely stereospecific, and no H/D exchange could be observed. Finally, Groves et al.[15] concluded that epoxidation of cyclohexene proceeds without an intermediate.

While, in Figure 7, the lowest-energy transition states are correlated to the intermediates ^{2,4}**2-IV** and ^{2,4}**4-IV**, we cannot rule out the involvement of the Fe^{III} intermediates (see Figure 4). Indeed, since these intermediates, ^{2,4}**2-III(III′)** and ^{2,4}**4-III-(III′)**, are lower in energy than both ^{2,4}**TS1** and ^{2,4}**TS3**, it is likely that these transition states can serve all the intermediates. In fact, inclusion of solvation (see Table 3) condenses the energy difference between the intermediates, and increase of medium polarity (e.g., the presence of water) will further condense these

(52) Audergon, C.; Iyer, K. R.; Jones, J. P.; Darbyshire, J. F.; Trager, W. F. *J. Am. Chem. Soc.* **1999**, *121*, 41.
(53) Fretz, H.; Woggon, W.-D. *Helv. Chim. Acta* **1986**, *69*, 1959.
(54) Fretz, H.; Woggon, W.-D.; Voges, R. *Helv. Chim. Acta* **1989**, *72*, 391.

differences, so that in practice all of them may become available. Thus, past the bond-activation phase there could exist multistate reactivity where LS intermediates have much smaller lifetimes than HS intermediates. Experimental evidence[55,56] indicates that these intermediates indeed coexist both in hydroxylation and in epoxidation and that this depends on the indentity of the proximal ligand and the polarity of the medium.

4.2. Factors Affecting Competition of Epoxidation and Allylic Hydroxylation. Experimentally, propene itself undergoes only epoxidation by $P450_{LM2}$,[23] while other simple alkenes such as 2-butenes,[22] cyclohexene,[13,15] unsaturated fatty acid,[18] and so forth exhibit both epoxidation and allylic hydroxylation. It was surmised that substrate binding and conformation play an important role in directing the regioselectivity of the reactions.[1b,18,57] For example, the half-chair conformation of cyclohexene,[13,15] produces overlap of the scissile C−H bond and the π-bond and exhibits both epoxidation and allylic hydroxylation, while cyclooctene which has a different conformation shows typically very little, if any, allylic hydroxylation.[16] Furthermore, in the case of cyclohexene, hydroxylation and epoxidation appear to proceed from different complexes which involve different interaction modes of cyclohexene with the FeO moiety.[15] In cases where the bond activation processes (hydroxylation or epoxidation) by Cpd I are very fast, the substrate binding mode will determine the regioselectivity and will mask the intrinsic factors. As may be seen later (Figure 8) the barriers for propene oxygenation are quite small, and the regioselectivity of its enzymatic oxidation may well be dominated by substrate-binding effects. Indeed, the fact that propene undergoes exclusively double bond epoxidation by $P450_{LM2}$,[23] may reflect the preferred mode of propene binding in the protein pocket. Our study does not include substrate-binding effects, and therefore it should be considered as a model investigation of the intrinsic factors affecting the regioselectivity of oxidation.

As the bond-activation phase for the two processes has larger barriers than the subsequent rebound step, we shall focus on the C−H versus C═C bond-activation barriers in Figure 7, as the determinants of the competition. Useful reference quantities are the corresponding barriers in ethene epoxidation (13.9 (HS) and 14.9 (LS) kcal/mol) and methane hydroxylation (26.7 (HS) and 26.4 (LS)). According to Scheme 4, the bond activation is attended by single-electron shifts from the reactive moiety of the substrate into the singly occupied orbitals of Cpd I. Thus, although this is a formal shift, still a significant amount of charge transfer from the substrate to the Cpd I moiety will be manifested in the transition state. It is expected therefore, *that as the substrate becomes a better electron donor, the barriers for bond activation should decrease*. Indeed, it is seen that both barriers in the case of propene are lower than the reference barriers, since both the C═C and C−H moieties of propene are better electron donors than the reference substrates. However, while the epoxidation barrier is reduced moderately by ca. 4 kcal/mol, the hydroxylation barrier changes three times as much. Moreover, starting with a difference of 12 kcal/mol in favor of epoxidation in the reference systems, in the case of propene the difference is reduced to only 3.5 kcal/mol. This large sensitivity of hydroxylation arises because the allylic C−H bond is weaker than an alkanyl C−H by ca. 16 kcal/mol. Consequently, the reaction driving force for C−H activation, which is highly endothermic in the case of methane,[27] becomes weakly exothermic for propene. In contrast, the reaction driving force of C═C activation in propene changes only slightly compared with the case of ethene.[30] As a result of these factors, the barrier to allylic hydroxylation is higher than that for C═C epoxidation by only 3.5 kcal/mol. With this small difference in the relative energies, the outcome of the competition can be determined by perturbations of other factors.

Zero-Point Energy Effect. The parenthetical numbers in Figure 7 are relative energies of the transition states for epoxidation and hydroxylation with zero-point energy (ZPE) correction. It is seen that the addition of ZPE brings all the bond activation barriers closer to within less than 1 kcal/mol, with some minor preference for epoxidation. The data in Table 2 show that the enthalpic barriers and the free energies of activation maintain this proximity that is set by the ZPE. Since the free energy is sensitive to very low-frequency modes, its accuracy may be questionable, and we prefer to base all further arguments on the *E* vis-à-vis *E*+ZPE scales.

The ZPE effect originates in the loss of the high-frequency C−H mode that becomes imaginary in the hydroxylation transition states, **TS3** (see Table S.12), while in the epoxidation transition states nothing of this magnitude happens (the C═C vibration becomes a C−C vibration). As a result, on the *E*+ZPE scale, the hydroxylation barrier is decreased by ca. 2.3−2.9 kcal/mol, while the epoxidation barrier is hardly affected (see Figure 7 and Table 2). Taken together, the donor ability of the reacting moiety, the bond energy of the bond undergoing activation, and the ZPE differences make allylic hydroxylation competitive with epoxidation. This competitiveness is perhaps manifested in the oxidation of cyclohexene, where the C═C/C−H ratio was found to be quite sensitive to changes in ligand, temperature, isotopic substitution, etc.[1a,4,13,15]

Hydrogen Bonding and Polarity Effects. Figure 8 shows the relative energies when two NH- - -S bonds are present. The values out of parentheses refer to energy only, while values in parentheses correspond to the *E*+ZPE scale. Comparison with the gas-phase data in Figure 7 reveals two noticeable effects. One concerning the rebound barriers shows that the hydrogen bonding to the thiolate raises the rebound barrier in epoxidation and lowers it in hydroxylation compared with the gas-phase barriers. However, a more intriguing effect occurs in the bond-activation phase, where NH- - -S hydrogen bonding lowers the LS barriers, while it has a smaller effect on the HS barriers. Furthermore, the effect is large on the hydroxylation barriers, to such an extent that the LS hydroxylation process attains the lowest barrier (*E*+ZPE) by a significant margin. The two hydroxylation barriers on the *E*+ZPE scale are very small, showing that Cpd I is made a more powerful hydroxylating agent partly due to the presence of two NH- - -S hydrogen bonds away from the reaction center, as present in the protein pocket.[58,59]

To visualize all the effects on a single scale, we summarize in Figure 9 the relative energies of the four bond-activation transition states under various conditions, initially (i) and (ii)

(55) Groves, J. T.; Gross, Z.; Stern, M. K. *Inorg. Chem.* **1994**, *33*, 5065.
(56) Gross, Z.; Nimri, S.; Barzilay, C. M.; Simkhovich, I. *J. Bioinorg. Chem.* **1997**, *2*, 492−506.
(57) Devos, J. J.; Sibbeseb, O.; Zhang, Z.; Ortiz de Montellano, P. R. *J. Am. Chem. Soc.* **1997**, *119*, 5489−5498.

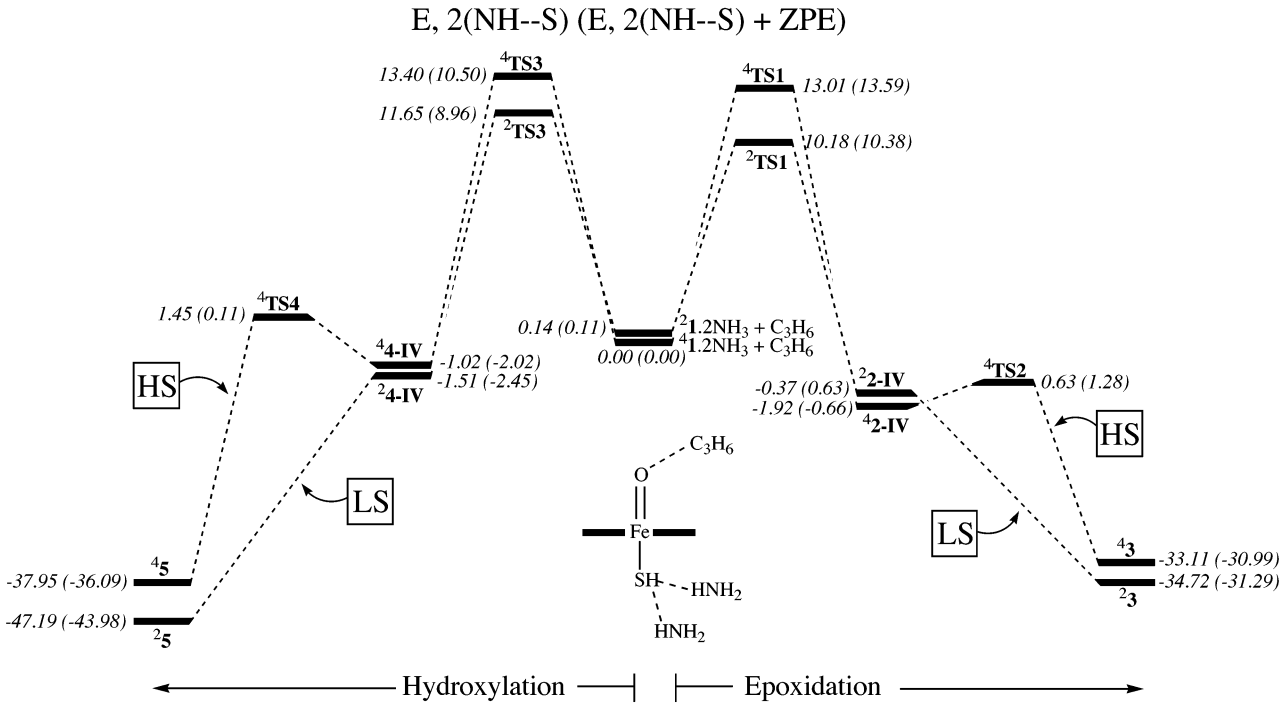

Figure 8. The effect of two NH- - -S hydrogen bonds on the lowest-energy pathways of allylic hydroxylation and epoxidation of propene by Cpd I. Values out of parentheses are energy only (E, 2(NH- -S)), while values in parentheses include zero-point energies (E, 2(NH- - -S)+ ZPE). ZPEs are calculated with Gaussian 98.

in the gas phase at the energy-only (E) and E+ZPE scales, followed by environmental effects; hydrogen bonding (iii), polarizing medium characterized by a dielectric constant of 5.7 (iv), and the combination of the latter two effects (v). Thus, relative to the gas phase, the addition of two NH- - -S hydrogen bonds (iii) causes a clear preference for the LS hydroxylation species, ^{2}**TS3**. A polarizing medium, in (iv) prefers both HS and LS hydroxylation species to epoxidations. Finally, combination of the effects, in (v), leads to a clear preference for the hydroxylation mechanism, where the LS ^{2}**TS3** lies below ^{2}**TS1** by as much as 3 kcal/mol. *It follows therefore that environmental effects of the type present in the protein pocket*[58,59] *reverse the regioselectivity of the reaction from a slightly favorable epoxidation to a clearly dominant hydroxylation, by more than 2 orders of magnitude*.

The environmental factors are seen to prefer clearly the LS transition states for both hydroxylation and epoxidation processes. Assuming that due to slow spin crossover, the LS and HS pathways will occur independently, then the preference of the LS processes, which are effectively concerted, will be expressed as an increased stereoselectivity. If we ignore spin-crossover effects initially as well as at the stage of the intermediates and simply consider energy differences between the bond activation transition states, we can then estimate that at 300 K, only 10% of the hydroxylation reaction will proceed via the HS transition state, ^{4}**TS3**, while less than 1% of the epoxidation will proceed via the corresponding HS species, ^{4}**TS1**. While these are rough considerations, still they highlight that the polarity and hydrogen bonding capability of the protein pocket can *exert a remarkable effect on the regioselectivity and stereoselectivity of the reaction*.

The calculated ease of allylic C−H hydroxylation is in accord with the opinion that the thiolate ligand endows the P450 enzymes with the ability to carry out hydroxylations of nonactivated C−H bonds.[3,4,16] The calculations show, however, that this function is intensified by the NH- - -S bonding machinery and the electric field of the protein. In line with the preference of the effectively concerted LS mechanism, via ^{2}**TS3**, experimental data show that alkane hydroxylations by P450 isozymes occur with high degrees of stereoselectivity, albeit incomplete, in the range of 90%.[1a,3,4,47] Similarly, epoxidations of *cis*- and *trans*-butenes by a few P450 isozymes were shown[22] to be stereospecific. An experimental study[20] that addresses the effect of NH- - -S hydrogen bonding on the ratio of C−H hydroxylation to C=C epoxidation, shows that in $P450_{cam}$ two hydrogen bonds are slightly more favorable for hydroxylation than three. This result is not directly comparable to our calculations, since we considered only two hydrogen bonds vis-à-vis none. In addition, another study by the same group[21] shows that changes in the hydrogen-bonding situation of the enzyme has adverse effects on the integrity of the complex. Nevertheless, the results of Morishima et al.[20] show that the NH- - -S hydrogen bonds apply a subtle effect on the reaction center and tune its selectivity patterns.

4.3. A Valence Bond Model for a Transition State of a Chameleon Oxidant. The calculations represent a first-principle demonstration of the existence of a significant electronic component that modulates the regioselectivity of C−H hydroxylation vis-à-vis C=C epoxidation. To understand the origins of this effect, we construct in this section a valence bond (VB) model for the transition states of the reaction.[60] Our VB model has

(58) Poulos, T. L.; Vickery, J. C. In *Cytochrome P450: Structures, Mechanism and Biochemistry*, 2nd ed.; Ortiz de Montellano, P. R., Ed.; Plenum Press: New York, 1995; Chapter 4, p 125−150.
(59) Schlichting, I.; Berendzen, J.; Chu, K.; Stock, A. M.; Maves, S. A.; Benson, D. E.; Sweet, R. M.; Ringe, D.; Petsko, G. A.; Sligar, S. G. *Science* **2000**, *287*, 1615.
(60) Shaik, S.; Shurki, A. *Angew. Chem., Int. Ed.* **1999**, *38*, 586−625.

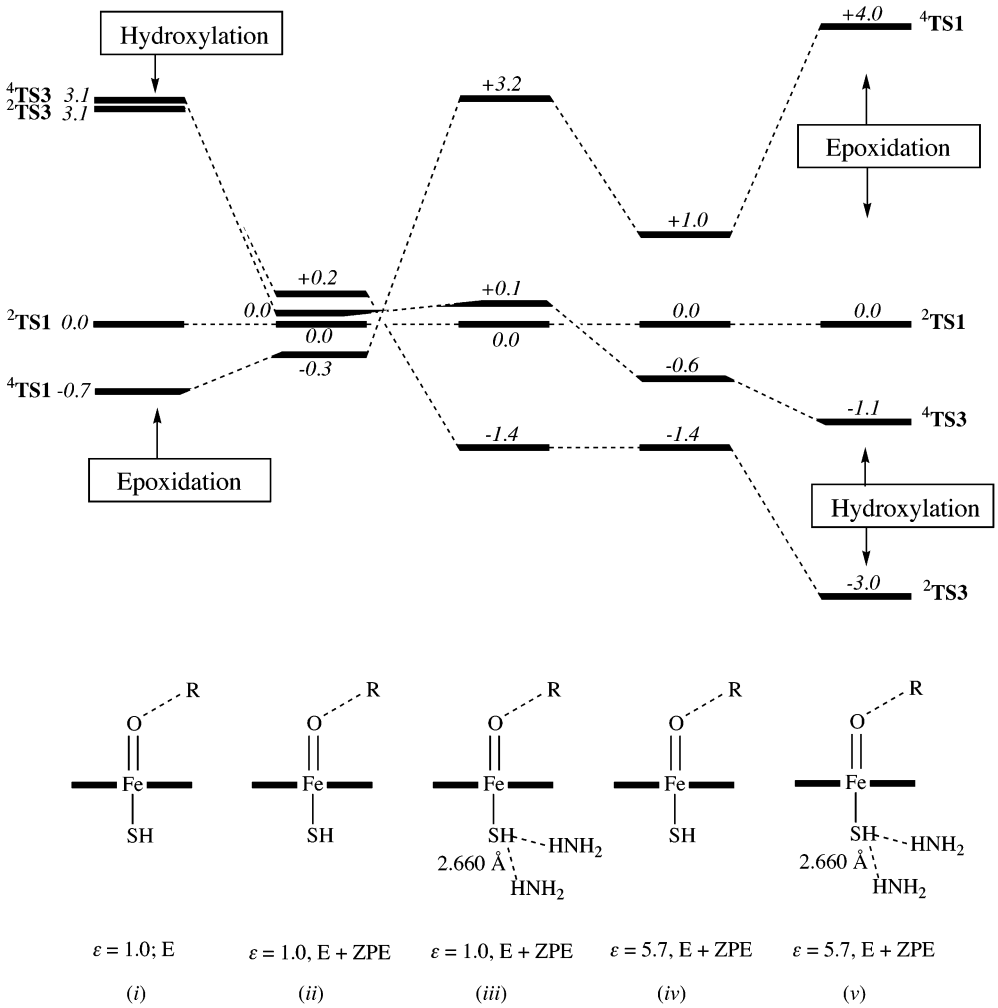

Figure 9. Relative energies of bond activation transition states for epoxidation and hydroxylation under different conditions: (i) in the gas phase, energy only, (ii) in the gas-phase E + ZPE, (iii) E+ ZPE with two NH- - -S hydrogen bonds, (iv) E + ZPE in a medium with dielectric constant, $\epsilon = 5.7$, (v) E + ZPE in a medium dielectric constant, $\epsilon = 5.7$, and with two NH- - -S hydrogen bonds.

affinity with the ideas of "redox mesomerism"[17] and "push effect"[3,61] that have been invoked[1a,4,62−66] to discuss the nature of Cpd I in P450 and the properties of the enzyme as a whole.

Initial insight into the electronic structure and its mutability can be gained from the data in Figure 10. Here we show the four transition states along with their spin density distribution, their degree of charge transfer, dipole moments, and average polarizabilities (more complete data are summarized in Tables S.1−S.10 and S.13). The epoxidation species (**TS1**) possess larger dipole moments compared with the hydroxylation counterparts (**TS3**). However, the relative energy changes imparted by the environmental factors (Figure 9) do not conform to the relative dipole moments of the TSs. Clearly, therefore, it is not a static property of the transition states that dictates the unique relative response to the environmental interactions. Indeed, a more suitable property seems to be the average polarizability which is higher for the hydroxylation transition states. Moreover, for each variety, it is the LS species that has the higher polarizability. This is in good qualitative accord with the calculated energy changes of these transition states in Figure 9. Thus, the environmental effects, described in Figures 8 and 9, exert their influence on the transition structures in the order of their polarizabilities, such that the most polarizable species ^{2}**TS3** is stabilized more than all other species, followed by ^{4}**TS3** and then ^{2}**TS1**. The HS epoxidation species, ^{4}**TS1** that has the smallest polarizability, is affected the least.

Polarizability is a dynamic property that reflects the mutability of the electronic structure under the influence of an external field.[67,68] Figure 10 shows spin density (ρ) data that characterize the electronic structures of the TSs. The data show that the LS transition states have less than two spins on iron ($\rho = 1.69$ and 1.73). Since the d orbital is doubly filled, the LS transition states approach an Fe^{IV} oxidation state with d^4 configuration. On the other hand, the HS transition states have slightly more than unit

(61) (a) Dawson, J. H. *Science* **1988**, *240*, 433−439. (b) Dawson, J. H.; Sono, M. *Chem. Rev.* **1987**, *87*, 1255−1276.
(62) Bangcharoenpaurpong, O.; Champion, P. M. *J. Chem. Phys.* **1987**, *87*, 4273−4284.
(63) Champion, P. M. *J. Am. Chem. Soc.* **1989**, *111*, 3433−3434.
(64) Unno, M.; Christian, J. F.; Benson, D. E.; Gerber, N. C.; Sligar, S. G.; Champion, P. M. *J. Am. Chem. Soc.* **1997**, *119*, 6614−6620.
(65) Weiss, R.; Mandon, D.; Wolter, T.; Trautwein, A. X.; Muther, M.; Eckhard, B.; Gold, A.; Jayaray, K.; Terner, J. *J. Bioinorg. Chem.* **1996**, *1*, 377−383.
(66) Weiss, R.; Mandon, D.; Bulach, V.; Gold, A.; Terner, J.; Trautwein, A. X. *J. Bioinorg. Chem.* **2001**, *6*, 831−845.
(67) A pioneering study of the effect of the protein's electric field on the resting state of P450 is: Harris, D. L.; Loew, G. H. *J. Am. Chem. Soc.* **1993**, *115*, 8775−8779.
(68) Aissaoui, H.; Bachmann, R.; Shweiger, A.; Woggon, W.-D. *Angew. Chem., Int. Ed.* **1998**, *37*, 2998−3002.

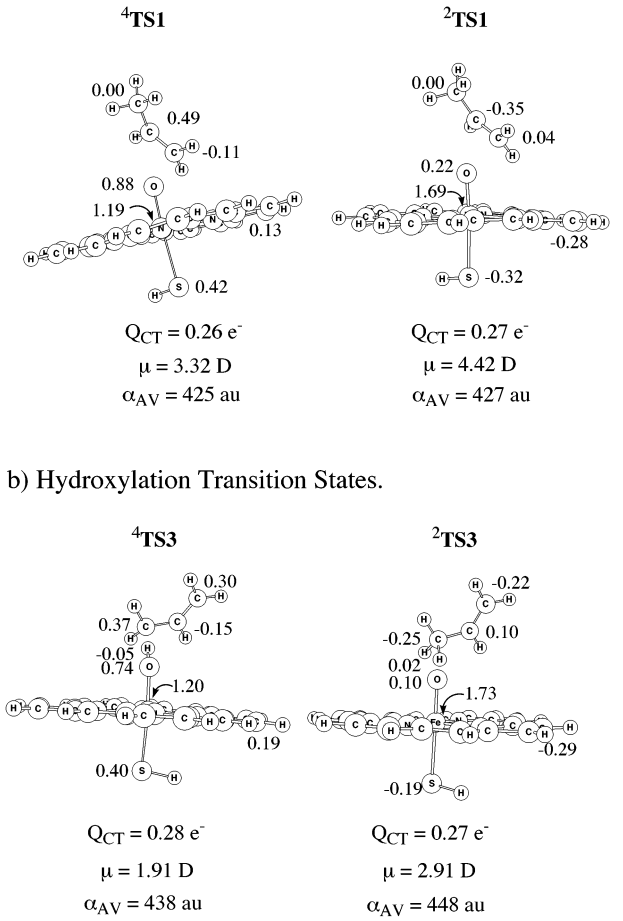

Figure 10. Group spin-density distribution in the bond-activation transition states. Below the structures are listed transition-state properties: Q_{CT} is the charge transfer from propene to the iron−oxo porphyrin moiety in electron units (e^-), μ is the dipole moment of the transition state in Debye units (D), and α_{AV} is the average polarizability of the transition state in atomic units (au).

spin ($\rho = 1.19$ and 1.20) located on the metal and are therefore closer to an Fe^{III} with a d^5 configuration. The fractional numbers of ρ(Fe) mean however, that both HS and LS transition states have mixed $Fe^{IV}-Fe^{III}$ characters to varying degrees and hence reflect different blends of the corresponding configurations. Another property of the transition state is Q_{CT}, which quantifies the amount of charge transfer from the propene to the iron−oxo complex. It is seen that about 0.3 of an electron is transferred in the transition states. It follows therefore that the transition states have a richly blended electronic character and mixed valent situations, which can give rise to high polarizability and sensitivity to environment effects.[67,68]

Two chemical properties are responsible for inducing a mutable character in the transition state. One is the donor ability of the thiolate ligand, and the second is the acceptor character of the iron porphyrin moiety that possesses quite a few low-lying half-filled orbitals. *This combination generates a few VB structures that are related by internal redox and are closely packed in energy, and therefore their contributions can be modulated by external factors*. Scheme 6 depicts these key VB structures. Here the propene is symbolized as R−G where G is the group that binds to the oxygen during the bond activation state (G = CH_2, H), while R represents the remaining part of the propene moiety that will carry the radical character in the transition state. Below each structure, we specify the idealized group spin densities (ρ), where the values in parentheses correspond to the LS situation, while those out of parentheses to the HS situation. There are six configurations that are common to the HS and LS transition states and an additional two that correspond only to the LS situations.

Structures |**a**> and |**b**> describe the contribution of the reactant state (Cpd I + propene) to the transition states. As shown recently,[34,40] the electronic structure of Cpd I itself is a hybrid of the resonance structures |**a**> and |**b**>, and this character carries over to the transition states. Already here one can see the special role of thiolate relative to other ligands, for example, imidazole. Thus, |**a**> and |**b**> are close in energy since thiolate is a sufficiently powerful donor to donate an electron to the "hole" in the porphyrin radical cation. In contrast, for a ligand like imidazole structure |**b**> will be unimportant.[69−73] The proximity of |**a**> and |**b**> with thiolate as a ligand will create an opportunity for NH- - -S hydrogen bonding and a polarizing electric field to tune the relative contributions of the VB structures and to affect thereby the energy of the transition state.

VB structures |**c**>−|**e**> describe characters of the reaction intermediates of the Fe^{IV} variety, in structure |**c**>, and the Fe^{III} variety, in |**d**> and |**e**>. These latter two structures again reflect the participation of thiolate as an electron donor to the electron-deficient centers in the iron porphyrin moiety. The structures labeled as |$\mathbf{d}_{LS}$> and |$\mathbf{e}_{LS}$> are equivalent to |**d**> and |**e**> but occur only in the LS variety. Finally, structure |**f**> describes the putative carbocation intermediate, which arises by charge transfer from the propene to the Cpd I moiety. It is drawn only in its HS configuration (corresponding to the $\pi^*_{xz}{}^1\ \pi^*_{yz}{}^1\ \sigma^*_{z^2}{}^1$ configuration on Fe^{III}), but there also exists a structure for the LS manifold with spin density of 1 on iron (corresponding to the $\pi^*_{xz^2}\ \pi^*_{yz}{}^1$ configuration on Fe^{III}). There are other charge-transfer structures, in which the sulfur appears both as thiolate (S^-) and thiolyl (S•), but they are not shown for reasons of space economy. The importance of these charge-transfer structures, |**f**>, will depend on the donor ability of the substrate, such that different substrates will endow the transition states with a charge-transfer character that matches their donation property. In addition, the importance of the charge-transfer structures will be modulated by the proximal ligand. Hydrogen bonding to the thiolate and medium polarization will make the iron porphyrin moiety a better electron acceptor[71b] and will therefore increase the role of the charge-transfer structures. Replacement of the thiolate ligand by a lesser electron donor like imidazole will have a similar effect.[3, 61,70.71b]

Our recent investigations[34,40] of Cpd I showed that in gas-phase conditions, Cpd I is |**b**>-like with a thiolate radical character (ca 54−70%), while medium polarization and NH- - -S hydrogen bonding stabilize structure |**a**> and endow Cpd I with a dominant porphyrin (Por) radical cation character (ca

(69) Loew, G. H.; Harris, D. L. *Chem. Rev.* **2000**, *100*, 407−419.
(70) Kuramochi, H.; Noodleman, L.; Case, D. A. *J. Am. Chem. Soc.* **1997**, *119*, 11442−11451.
(71) (a) Filatov, M.; Harris, N.; Shaik, S. *J. Chem. Soc., Perkin Trans. 2* **1999**, 399−410. (b) Ogliaro, F.; de Visser, S. P.; Shaik, S. *J. Inorg. Biol.* **2002**, in press.
(72) Green, M. T. *J. Am. Chem. Soc.* **2000**, *122*, 9495−9499.
(73) Harris, D. L.; Loew, G. H. *J. Porphyrins Phthalocyanins* **2001**, *5*, 334−344.

Scheme 6. Valence Bond Structures for the Description of the Transition States of Oxygenation by Cpd I[a]

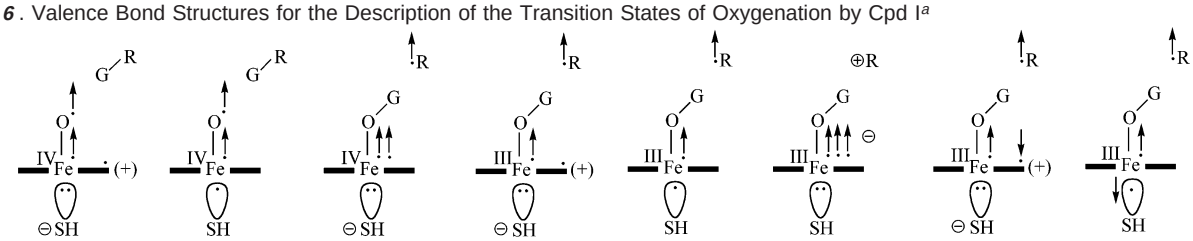

		a>		b>		c>		d>		e>		f>		d_{LS}>		e_{LS}>
ρ(O)	= 1	1		0		0		0		0		0		0	
ρ(Fe)	= 1	1		2		1		1		3 (1)		1		1	
ρ(Por)	= 1 (-1)	0		0		1 (-1)		0		0		-1		0	
ρ(SH)	= 0	1 (-1)		0		0		1 (-1)		0		0		-1	

HS and LS — LS-only

		Δμ (gas-phase -> 2NH--S)
Epoxidation:	^{4}**TS1** (^{2}**TS1**)	0.88 (1.04) D
Hydroxylation:	^{4}**TS3** (^{2}**TS3**)	0.34 (1.62) D

[a] The ρ values underneath each structure are the idealized group spin densities, for the HS (out of parentheses) and the LS (within parentheses). Shown below are also changes in the dipole moments (Δμ, in Debye units) of the transition states due to NH- -S hydrogen bonding.

70−75%). The stronger the hydrogen bonding and the polarizing effect are, the more |**a**>-like would Cpd I be. This chameleonic character carries over to the transition state that, in turn, possesses a variety of other VB structures and becomes a chameleon species itself through the change in its VB blend in response to the interactions with the environment.

The calculations reflect this chameleonic behavior through many small but significant changes in the group spin densities, charges, and amounts of charge transfer of the transition states in their "naked" gas-phase situations vis-à-vis their situations with environmental effects. There is no obvious way to relate these many changes quantitatively to specific changes in the VB contributions. It is possible however to appreciate this chameleonic behavior by looking at global changes in the electron density. At the bottom of Scheme 6, we summarize the dipole moment changes (Δμ) of the transition states upon transfer from the gas phase to the situation with two NH- - -S hydrogen bonds. These changes reflect the relative changes in the electron density distribution in the transition states upon NH- - -S hydrogen bonding and hence account globally for the changes in the corresponding VB-blends. It is seen that the two LS transition states undergo larger changes compared with their HS counterparts. Further, the largest change is exhibited by the LS hydroxylation species, ^{2}**TS3**, which undergoes the largest stabilization by the environmental effects (see Figure 9). These changes mirror the computed energy changes in Figure 9 and support the notion that these transition states behave like chameleon species.

The VB model of the chameleonic transition states allows gaining some insight into the computational results. First, it is seen in Scheme 6 that the LS states have more available VB structures, and one may, therefore, surmise that this is the reason the LS species are more highly affected by the environmental factors compared with their HS counterparts. Second, the calculations show that significant changes in the transition-state spin densities occur across the newly formed bonds, O- - -C and O- - -H, and especially in the LS species (Tables S.1 and S.4). Thus, the O- - -C and O- - -H bonds in the LS transition states almost entirely lose their net spins when NH- - -S hydrogen bonding and polarization effects are present. For example, by adding two NH- - -S bonds to ^{2}**TS3** and ^{2}**TS1**, the O- - -H spin densities change from 0.10/0.02 to 0.03/0.02, and the O- - - -C spins change from 0.22/0.04 to 0.00/0.06, respectively. This loss of spin density means that the newly formed bonds become almost fully spin-paired, as in structures |**c**>−|**f**>, |$\mathbf{d_{LS}}$>, and |$\mathbf{e_{LS}}$>, and thereby stronger bonds. Since the O−H bond is intrinsically stronger than O−C, the energetic effect on the hydroxylation transition states is likely to be more pronounced as indeed observed in Figures 8 and 9. Thus, the chameleonic nature of the transition state for P450 enzymes has an energy expression, which in turn affects the regioselectivity and stereospecificity of the oxygenation reactions.

While thiolate gives rise to a chameleonic behavior, a lesser electron donor ligand such as imidazole does not possess this ability to participate in electron delocalization, and hence the oxygenation reactions of Cpd I species with imidazole are less likely to exhibit this chameleonic behavior unless the ligand participates in its ionic form (imidazolate). This is likely to be the reason imidazole-based Cpd I species, as in the enzyme horseradish peroxidase (HRP), in model systems perform epoxidations preferentially, whereas thiolate-based Cpd I species perform higher degrees of hydroxylations.[16] This can also be the reason behind the findings of Mansuy et al.,[12] that with ligands such as Cl^-, making the porphyrin moiety a better electron acceptor enhances the amount of C−H hydroxylation (see also review in ref 11). The changes noted by Groves et al.,[15] that the hydroxylation/epoxidation ratio (at −78 °C) of cyclohexene increases with the donor ability of the proximal ligand may also reflect the same reason, namely that with the better electron donor ligand, a chameleon transition state tends to prefer hydroxylation. Thus, while the VB model is still very

qualitative, it nevertheless gives a framework capable of explaining experimental findings.

Conclusions

The above study investigated the electronic factors that affect the epoxidation (C═C) vis-à-vis allylic hydroxylation (C−H) reactions of propene with compound I (Cpd I). The effects of external interactions such as NH- - -S hydrogen bonding to the thiolate ligand and polarization by an electric field of a nonpolar medium (with $\epsilon = 5.7$), were addressed. These interactions mimic, albeit naively, the electronic effects exerted in the protein pocket, on Cpd I and all species along the oxygenation pathways. It is found that the weakening of the allylic C−H bond relative to a C−H bond in a saturated alkane and the zero-point energy loss as the C−H bond is cleaved in the hydroxylation transition state, together make the epoxidation and hydroxylation processes competitive. Still, the bare molecules exhibit a small preference for epoxidation (C═C/C−H > 1).

A major impact on the C═C/C−H ratio is exerted by the environmental factors. Thus, *two NH- - -S hydrogen bonds away from the reaction center* are capable of reversing the regioselectivity ratio, C═C/C−H, and prefer hydroxylation. The polarity of the medium further accentuates the trend leading to a change of 2 orders of magnitude in the regioselectivity. These interactions also affect the stereoselectivity and are expected to render both processes more stereoselective by preferring the effectively concerted reactions of the low-spin (LS) states. It follows therefore that not only is Cpd I a chameleon species, *it is also a chameleon oxidant that tunes its reactivity and selectivity patterns in response to the protein environment in which it is accommodated*.

This unusual sensitivity is due to the donor ability of thiolate, which can donate electrons to the electron-poorer centers on the iron porphyrin moiety. A VB model of such a chameleon transition state (Scheme 6) shows how the donor−acceptor relationship of the thiolate and iron porphyrin give rise to a few extra VB structures that are related by internal redox and are closely packed in energy. This close packing of the VB structures and their polarized nature create transition states, which are tunable by NH- - -S bonding and electronic polarization effect within the protein pocket. Thus, *the enhanced ability of P450 enzymes to perform hydroxylations of C−H bonds is an emergent property that reflects the modulation of the thiolate donor ability by the specific protein environment.*

Our study is a first-principle demonstration that there is a significant electronic component that modulates the regioselectivity of oxidation by P450 enzymes. Within the protein pocket there also exist, however, classical factors of substrate fit, accessibility, and binding.[1a,1b,4,18,57] The ultimate regioselectivity will reflect the interplay of the electronic component with the classical factors. QM/MM calculations will eventually be required to elucidate the interplay of all the factors. Until then, since the present study does not consider the classical factors, the computed regioselectivity ratio, C═C/C−H > 1, can serve as a guide for an intrinsic regioselectivity. Great variations from this limit for a given substrate will indicate effects due to steric problems and substrate bindings. For example, the fact that $P450_{LM2}$ leads only to propene epoxidation[23] is such an indication that the substrate is bound through its double bond, and since the barrier is so small the substrate is consumed by the epoxidation path.

Finally, a comment on the two-state reactivity scenario (TSR) is in order. Despite the energy separation of the bond-activation transition states by the environmental effects (Figure 9), which prefers the LS processes, the reactions will still occur by TSR for two major reasons. First, due to the chameleonic nature of Cpd I, the third unpaired electron will be mainly in a porphyrin-based orbital. This will render the spin−orbit coupling interaction that can mix the HS and LS situations rather small, so that the two processes will proceed independently from the two states of Cpd I. Second, even though the HS and LS transition states are separated in energy at the transition state, at the intermediate stage, the HS and LS states are again almost degenerate, and both processes can be populated.

Acknowledgment. We thank the Israeli Science Foundation (ISF), the German-Israeli Binational Foundation (GIF), and the Ministry of Culture, Science and Sport for support. Discussions with J. T. Groves and A. D. N. Vaz are acknowledged.

Supporting Information Available: Sixteen tables with absolute energies, orbital occupations, group spin densities, group charges, and geometrical parameters of all compounds listed in the text; seven figures with scans of the various processes (PDF). This material is available free of charge via the Internet at http://pubs.acs.org.

JA026872D